

Genomic Adaptations to Salinity Resist Gene Flow in the Evolution of Floridian Watersnakes

Rhett M. Rautsaw^{1,2}, Tristan D. Schramer¹, Rachel Acuña², Lindsay N. Arick², Mark DiMeo^{1,2}, Kathryn P. Mercier^{1,2,3,4}, Michael Schrum², Andrew J. Mason^{1,2}, Mark J. Margres^{1,5,6}, Jason L. Strickland^{1,2,7}, and Christopher L. Parkinson^{1,2,8}

¹Department of Biological Sciences, Clemson University, 190 Collings St., Clemson, SC 29634, USA

²Department of Biology, University of Central Florida, 4000 Central Florida Blvd., Orlando, FL 32816, USA

³Department of Biology, City College of New York, 160 Convent Ave., New York, NY 10031 USA

⁴PhD Program in Biology, The Graduate Center of the City University of New York, 365 Fifth Ave., New York, NY 10016 USA

⁵Department of Organismic and Evolutionary Biology, Harvard University, Cambridge, MA 02138, USA

⁶Department of Integrative Biology, University of South Florida, Tampa, FL 33620, USA

⁷Department of Biology, University of South Alabama, Mobile, AL 36688, USA

⁸Department of Forestry and Environmental Conservation, Clemson University, 190 Collings St., Clemson, SC 29634, USA

Corresponding Author:

Christopher L. Parkinson

Email: viper@clemson.edu

ORCID:

Rhett M. Rautsaw: 0000-0002-8229-5951

Tristan D. Schramer: 0000-0002-4553-8002

Kathryn P. Mercier: 0000-0001-7898-1353

Andrew J. Mason: 0000-0003-0297-1313

Mark J. Margres: 0000-0002-6153-6701

Jason L. Strickland: 0000-0002-1927-7259

Christopher L. Parkinson: 0000-0002-2020-6992

© The Author(s) 2020. Published by Oxford University Press on behalf of the Society for Molecular Biology and Evolution.

This is an Open Access article distributed under the terms of the Creative Commons Attribution License

(<http://creativecommons.org/licenses/by/4.0/>), which permits unrestricted reuse, distribution, and reproduction in any medium, provided the original work is properly cited.

Abstract (250 words)

The migration-selection balance often governs the evolution of lineages, and speciation with gene flow is now considered common across the tree of life. Ecological speciation is a process that can facilitate divergence despite gene flow due to strong selective pressures caused by ecological differences; however, the exact traits under selection are often unknown. The transition from freshwater to saltwater habitats provides strong selection targeting traits with osmoregulatory function. Several lineages of North American watersnakes (*Nerodia* spp.) are known to occur in saltwater habitat and represent a useful system for studying speciation by providing an opportunity to investigate gene flow and evaluate how species boundaries are maintained or degraded. We use ddRADseq to characterize the migration-selection balance and test for evidence of ecological divergence within the *N. fasciata-clarkii* complex in Florida. We find evidence of high intraspecific gene flow with a pattern of isolation-by-distance underlying subspecific lineages. However, we identify genetic structure indicative of reduced gene flow between inland and coastal lineages suggesting divergence due to isolation-by-environment. This pattern is consistent with observed environmental differences where the amount of admixture decreases with increased salinity. Furthermore, we identify significantly enriched terms related to osmoregulatory function among a set of candidate loci, including several genes that have been previously implicated in adaptation to salinity-stress. Collectively, our results demonstrate that ecological differences, likely driven by salinity, cause strong divergent selection which promotes divergence in the *N. fasciata-clarkii* complex despite significant gene flow.

Keywords: ecological niche, introgression, local adaptation, selection, speciation

Introduction

Once thought to be rare, speciation with gene flow is now considered exceedingly common across the tree of life (Nosil 2008; Barth et al. 2020). Speciation genomics has uncovered evidence of rampant introgression among species and reticulate evolution of lineages, lending insights into how speciation progresses (Feder et al. 2012; Campbell et al. 2018; Mason et al. 2019). Although gene flow is typically considered a homogenizing force, reducing divergence among species and impeding local adaptation (Endler 1977; Slatkin 1987; Garcia-Ramos and Kirkpatrick 1997; Lenormand 2002), many cases exist in which gene flow promotes divergence by introducing genetic variation, or speciation proceeds in spite of gene flow (Slatkin 1987; Ingvarsson 2001; Garant et al. 2007; Lamichhaney et al. 2015; Pease et al. 2016; Pfeifer et al. 2018; Choi et al. 2019; Dean et al. 2019; Margres et al. 2019). Identifying the processes which underly speciation with gene flow is a key goal in evolutionary biology, but the interaction of evolutionary forces can be complex and vary dramatically across systems (Garant et al. 2007).

Strong selection caused by ecological differences between populations can lead to local adaptation and promote speciation (Schluter 2000; Rundle and Nosil 2005). If selection is weak, gene flow may result in genetic swamping whereby locally fit genotypes are driven to extinction. Alternatively, strong selection may overcome the homogenizing force of gene flow and maintain diversity or facilitate divergence. Therefore, migration and selection sit in a balance which governs the evolution of a given lineage (Haldane 1930; Wright 1931; Yeaman and Whitlock 2011; Savolainen et al. 2013; Tigano and Friesen 2016). Ecological speciation provides a set of predictions which can be explicitly tested with regards to gene flow and selection. Under ecological speciation, the effect of isolation-by-environment (IBE) should be greater than isolation-by-distance (IBD) since species are able to persist despite close proximity (Wang and Bradburd 2014). Detecting signatures of ecological speciation requires characterizing the migration-selection balance and ecological divergence in order to determine the prevalence of gene flow, characterize the ecological factors influencing divergence, and identify loci under selection that are resistant to the homogenizing effects of gene flow. Identifying historical or ongoing ecological speciation can therefore be more readily accomplished in systems where environmental conditions promote differential selection pressures on putatively divergent lineages.

The transition from freshwater to saltwater can provide strong divergent selection due to the physiologically-harsh, high-saline environment (Hong et al. 2019). For example, less than one percent of extant reptiles extensively utilize saltwater habitats (Rasmussen et al. 2011; Peng et al. 2020). In lineages that occur in saltwater, selection has targeted genes related to osmoregulatory function and ion transport (Zhang et al. 2017; Hong et al. 2019; Mansouri et al. 2019; Lee et al. 2020); therefore, lineages that occur in freshwater and saline environments provide an opportunity to study ecological speciation. At least four North American watersnake (*Nerodia* spp.) lineages are known to occur in high-salinity environments

(Rasmussen et al. 2011). Watersnakes are also widespread, abundant, and many lineages are sympatric—providing ample opportunity for gene flow, including inferred hybridization, and enabling the investigation of the formation, maintenance, and/or degradation of species boundaries (Conant 1963; Lawson et al. 1991; Mebert 2008). The *N. fasciata-clarkii* complex, in particular, is differentiated by only a few morphological characters and presumed ecological differences, with *N. fasciata* (Southern Watersnake) predominantly occupying—but not limited to—freshwater habitats and *N. clarkii* (Salt Marsh Snake) occupying coastal, mostly saltwater habitats (Lawson et al. 1991; see Gibbons and Dorcas 2004 for full distributions of each taxon; USFWS 2008). Moreover, unlike most marine reptiles, *N. clarkii* does not have salt glands and display no clear physiological adaptations to high salinity environments (Pettus 1958; Pettus 1963; Dunson 1980; Babonis et al. 2011). Despite this, *N. clarkii* is able to maintain its plasma ion balance more effectively than its sister species; therefore, the mechanisms that allow *N. clarkii* to maintain osmotic or ionic balance remain elusive (Babonis et al. 2011). Environmental and behavioral differences between *N. fasciata* and *N. clarkii* suggest local adaptation, but few studies have tested whether genetic or molecular differences occur between the two species (Lawson et al. 1991; Jansen 2001) and no studies have tested for an association between genetic variation and salinity tolerance.

Characterizing the migration-selection balance of the *N. fasciata-clarkii* complex also has critical implications for conservation biology. Within Florida, *N. fasciata* and *N. clarkii* are composed of five subspecies (*N. f. fasciata*, *N. f. pictiventris*, *N. c. clarkii*, *N. c. compressicauda*, and *N. c. taeniata*; fig. 1), with *N. c. taeniata* listed as a federally threatened subspecies (USFWS 2008). Previous research has questioned the separation of *N. fasciata* and *N. clarkii* because of low interspecific divergence and substantial morphological intergradation, hypothesized to be the result of high gene flow (Carr and Goin 1942; Lawson et al. 1991; USFWS 2008; reviewed in Territo 2013). The lack of clear morphological differentiation and hypothesized gene flow among lineages has made delineating conservation units and evaluating the recovery status of *N. c. taeniata* difficult (USFWS 2008), necessitating the use of genomics and current approaches to inform future decision making.

Given the ecologically divergent nature of the *N. fasciata-clarkii* complex, we hypothesize that adaptations to saline environments are able to resist the homogenizing effects of gene flow between *N.*

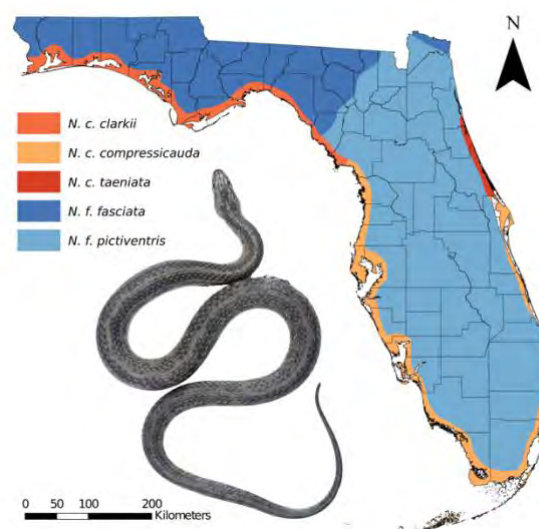


Fig. 1. Distribution map for the five subspecies within the *Nerodia fasciata-clarkii* complex in Florida. Colors are maintained throughout the manuscript. Photo of *N. c. taeniata* by G. Territo.

fasciata and *N. clarkii*. (Lawson et al. 1991). If adaptation facilitates differentiation in spite of gene flow, we expect to find genetic structure corresponding to environmental differences (*i.e.*, salinity) between *N. fasciata* and *N. clarkii*. Specifically, we expect the influence of IBE to outweigh patterns of IBD between species, but not between subspecies/populations within a species. Additionally, we expect to find evidence of ecological divergence among lineages and genomic signatures of selection associated with loci related to osmoregulatory functions. Therefore, we aim to (1) identify population structure and infer the evolutionary history of the group, (2) characterize the role of gene flow and hybridization in shaping these patterns, (3) test for ecological niche divergence and determine if genetic differentiation or admixture is related to niche differentiation, (4) identify loci under selection and determine if they are related to osmoregulatory function, and (5) evaluate the implications of our findings for conservation in light of the threatened status of *N. c. taeniata*. To do this, we use a combination of Sanger sequencing and double digest restriction-site associated DNA sequencing (ddRADseq) to infer population structure and phylogenetic history. We use the ddRADseq data and multiple analytical methods to provide evidence of gene flow, including hybrid lineage formation, and search for outlier loci associated with osmoregulatory function. We use publicly available environmental data, including soil cation exchange capacity as a proxy for salinity, to test for differences in ecological niche and ask whether salinity may be a driver for genetic differentiation or admixture between the species. Finally, we utilize several morphological characters to explore their utility in diagnosing species or subspecies within this complex. For ease, we utilize the existing nomenclature to communicate and discuss our results.

Results

Population Structure

To assess population structure, we performed ddRAD-Seq on 131 individuals including one outgroup (*Thamnophis saurita*). Our final filtered dataset consisted of 119 individuals (including the outgroup) and 7,057 SNPs. Excluding the outgroup, we identified population clusters using a discriminant analysis of principal components (*DAPC*; Jombart et al. 2010). K-means clustering identified K=6 as the best fit model with K=5 and K=7 performing similarly ($\Delta\text{BIC} < 2$; fig. supplementary fig. S1). We used all three models of population structure (*i.e.*, K=5, K=6, K=7) for downstream analyses. In addition, we examined the geographic structure at K=2 to assess if genetic clustering accurately represents the distribution of the two species (fig. 2A). At K=2, clustering followed a coastal/inland dichotomy similar to the approximate ranges of *N. clarkii* and *N. fasciata* (fig. 1 & 2A). Similarly, at K=5, the population clustering approximates the ranges of the five subspecies in Florida (fig. 1 & 2B). In addition to general concordance between the *DAPC* clusters and expected distributions of the species/subspecies (fig. 1 & 2), we also found that species assignment at capture had 92% concordance with K=2 *DAPC* clusters and

subspecies assignment had 88% concordance with $K=5$ *DAPC* clusters (ignoring the 7 individuals included in ddRAD-Seq sampling with uncertain taxonomic assignment; supplementary table S1) However, it should be noted that assignment at capture was not performed blind with respect to sampling location. Accordingly, we utilize the current taxonomy to refer to concordant genetic clusters to communicate the remainder of our results. At $K=6$ and $K=7$, only *N. c. compressicauda* was impacted (fig. 2C & 2D). At $K=6$, the best fit model, the southern portion of the range was separated from central Florida populations, followed by separation of the east and west coasts at $K=7$ (fig. 2C & 2D).

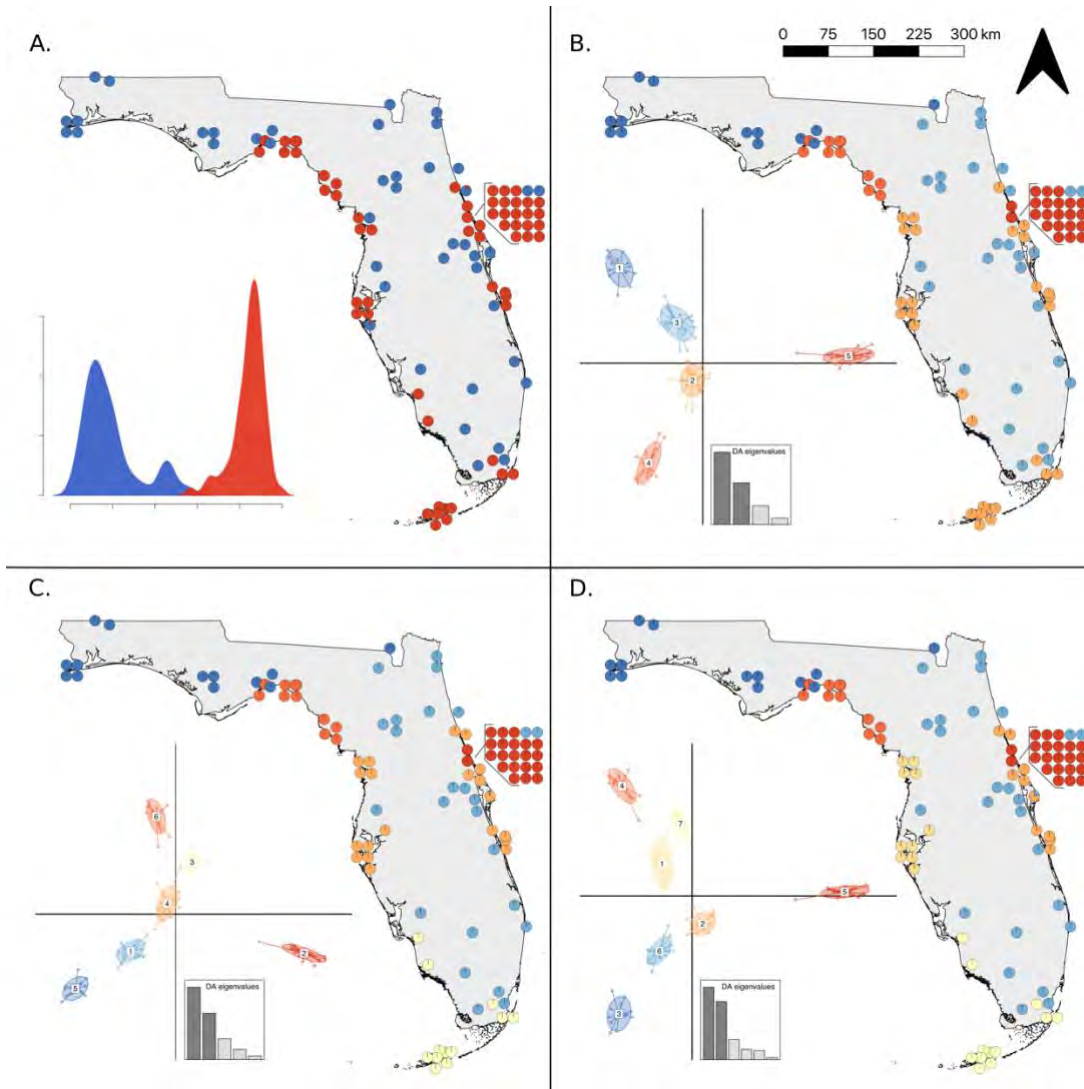


Fig. 2. *DAPC* population structure for 118 snakes across Florida. (A) $K=2$ shows that genetic clustering is similar to the species distributions (see fig. 1). Population structure at (B) $K=5$ shows that genetic clustering is similar to subspecies distributions (see fig. 1). The best supported *DAPC* model, (C) $K=6$, separates the *N. c. compressicauda* population into central and southern groups. (D) At $K=7$, the eastern and western *N. c. compressicauda* clades separate. Inset density and scatter plots represent separation along discriminant axes and the DA eigenvalues describe how much discriminating ability the model possesses. Not all 118 points may be visible in maps since some points overlap.

To dissociate population structure from continuous clines of genetic variation, we ran *conStruct* (Bradburd et al. 2018). Cross-validation analysis in *conStruct* found that spatially-aware analyses outperformed non-spatial analyses, suggesting that some divergence in the *N. fasciata-clarkii* complex can be attributed to isolation-by-distance (supplementary fig. S2). We examined the contribution of each additional layer (K) and found that the majority of the data are explained with two layers, suggesting that there are two significantly different isolation-by-distance clines in our data (K=2; supplementary fig. S2). Geographic structure of these data followed the coastal-inland dichotomy previously identified by *DAPC* (K=2) and was similar to the species ranges of *N. clarkii* and *N. fasciata* (fig. 1 & 3A). *conStruct* also identified high admixture proportion between the two species, with *N. clarkii* frequently having upwards of 50% admixture from *N. fasciata* (fig. 3A); however, there was little evidence of admixture within *N. fasciata* from *N. clarkii* (fig. 3A). The high admixture proportion detected in *N. clarkii* but not *N. fasciata* could be due to unidirectional gene flow, shared ancestral polymorphism, or differences in effective population size (Lawson et al. 2018). Nonetheless, we identified substantial allelic variation unique to *N. clarkii*, which highlights the shared ancestry of coastal lineages as well as their genetic distinction from *N. fasciata*.

Phylogenetics

Initial phylogenetic analysis of the mitochondrial gene, *cytb*, for 268 individuals and 20 outgroups found no support for subspecies or species monophyly (supplementary fig. S3). Further analysis with two additional mitochondrial genes (*ND1* and *ND4*), two nuclear genes (*PRLR* and *TATA*), and two anonymous loci (*M* and *E*) for 85 individuals and 11 outgroups confirmed these results. Overall, single-gene sequencing provided little resolution within the *N. fasciata-clarkii* complex with large polytomies, low support, and the only clear distinction occurring between continental and peninsular populations (supplementary fig. S3) as

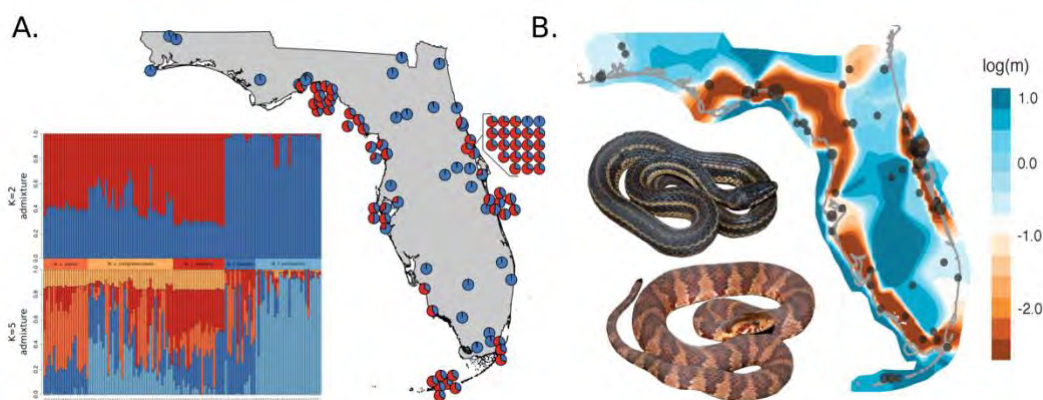


Fig. 3. (A) *conStruct* population structure and admixture at K=2 with additional K=5 admixture plot showing little structure at K=5. (B) Estimated effective migration surface (*EEMS*) for the *N. fasciata-clarkii* complex. High migration is represented by shades of blue; low migration is represented by red-orange shades. *EEMS* demonstrates increased gene flow within and decreased gene flow between the coastal and inland populations. Photos of *N. c. clarkii* and *N. f. fasciata* by K. Wray.

is commonly seen in taxa with similar distributions (Soltis et al. 2006; Strickland et al. 2014; Margres et al. 2019).

To assess the phylogenomic history of the group, we generated a bi-allelic SNP alignment and used *SVDquartets* (Chifman and Kubatko 2014). The resulting phylogeny demonstrated strong support for several monophyletic clades generally corresponding to the *DAPC* clusters (fig. 4). Primarily, a lineage of individuals, all but one of which were identified as *N. f. fasciata* at capture and by *DAPC*, were found to be sister to the remaining taxa. Following this, a branching event led to a lineage corresponding to *N. f.*

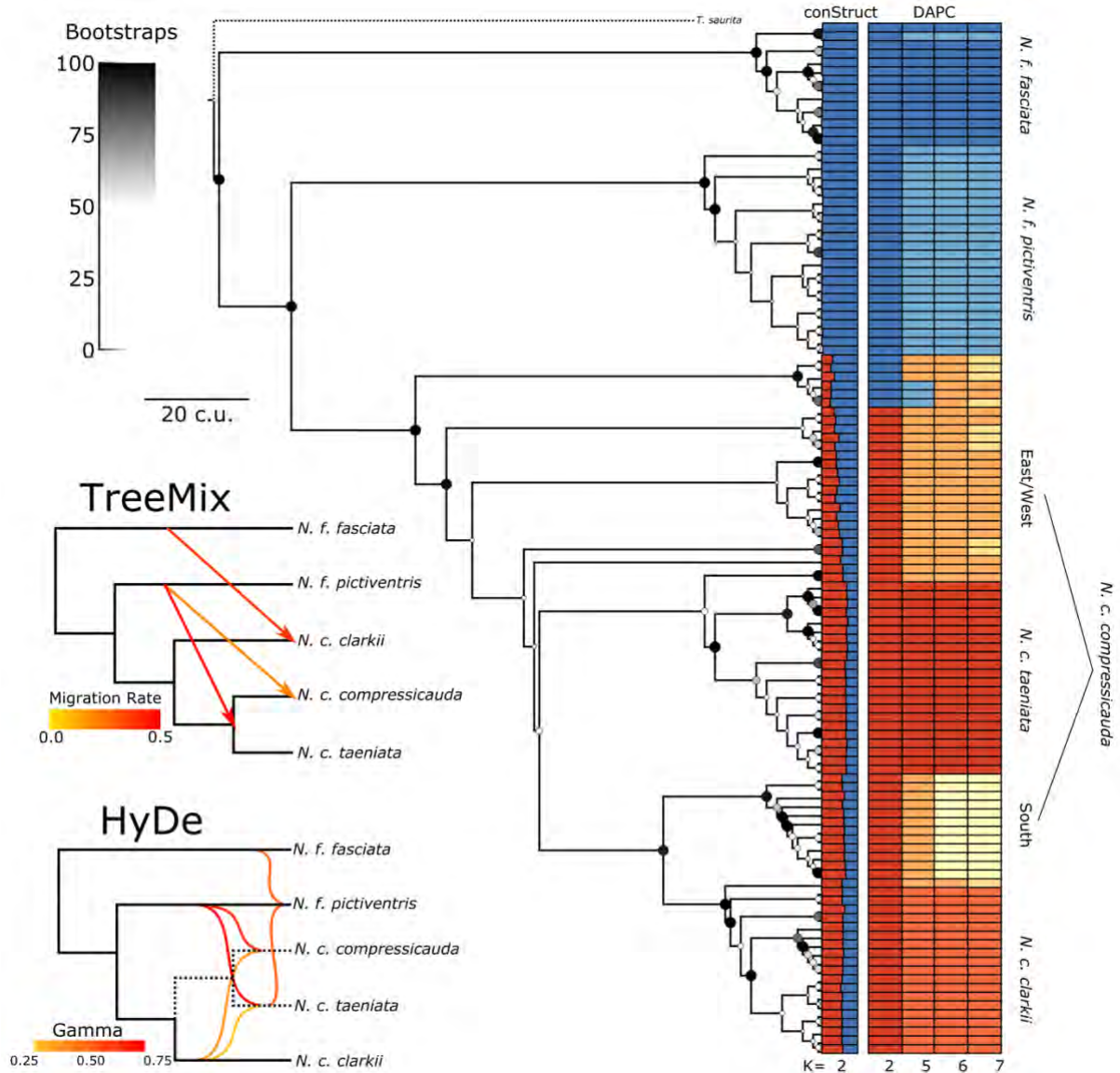


Fig. 4. *SVDquartets* inferred phylogeny with *conStruct* and *DAPC* results annotated. Nodal support is represented by color and size with large, black dots representing 100% bootstrap support and small, white points representing 0%. See supplementary fig. S7 for a cladogram with numerical support values. *SVDquartets* and *Treemix* species tree are also shown for $K=5$ with three migration edges leading from *N. f. fasciata* to *N. c. clarkii*, particularly from *N. f. pictiventris* to *N. c. compressicauda*. *HyDe* similarly detected three significant hybridization events, position of hybridization edges on branches is arbitrary.

pictiventris, rendering *N. fasciata* paraphyletic (fig. 4). Sister to *N. f. pictiventris*, is a large clade of individuals with high admixture proportion as inferred by *conStruct* (fig. 4). Six individuals with ambiguous *DAPC* assignments and with 63–74% *conStruct* admixture proportions from *N. fasciata* form the sister clade to individuals consistently assigned to *N. clarkii*. Within the *N. clarkii* clade, several branching events occur associated with the central *N. c. compressicauda* *DAPC* cluster, rendering this cluster paraphyletic (fig. 4). These small, paraphyletic clades generally have low support (<50%) and could be the result of a hard polytomy or admixture from *N. fasciata* (fig. 4). Sister to the paraphyletic clades corresponding to central *N. c. compressicauda*, is a moderately supported split leading to a clade consisting of *N. c. taeniata*, *N. c. clarkii*, and southern *N. c. compressicauda* (fig. 4). However, three individuals assigned to central *N. c. compressicauda* were also found sister to either the *N. c. taeniata* or *N. c. clarkii* clades, further demonstrating their uncertain phylogenetic placement and paralogy of *N. c. compressicauda*.

In addition, we used the K=5, K=6, and K=7 *DAPC* clusters to construct species trees with *SVDquartets*. All three species trees had 100% bootstrap support for all nodes. The K=5 tree similarly identified *N. f. fasciata* as sister to the remaining taxa followed by a branching event leading to *N. f. pictiventris* and *N. clarkii* (fig. 4). Within *N. clarkii*, *N. c. clarkii* was found to be sister to a branching event of *N. c. compressicauda* and *N. c. taeniata* (fig. 4). At K=6 and K=7, central *N. c. compressicauda* was found sister to the remaining *N. clarkii* clade (supplementary fig. S4).

Gene Flow

To test for migration events in the evolutionary history of the Florida *N. fasciata-clarkii* complex, we ran *Treemix* (Pickrell and Pritchard 2012) on the *DAPC* cluster assignments at K=5, 6, and 7. The best network at K=5 matched the species tree inferred by *SVDquartets*, but contained three migration edges suggesting gene flow from *N. fasciata* into *N. clarkii* (fig. 4). One migration edge led from *N. f. fasciata* to *N. c. clarkii*, one migration edge was inferred from *N. f. pictiventris* to the base of *N. c. taeniata* and *N. c. compressicauda*, and one migration edge was inferred from *N. f. pictiventris* directly to *N. c. compressicauda* (fig. 4). At K=6, the best network did not match the *SVDquartets* species tree, but also contained three migration edges; one leading from *N. f. pictiventris* to *N. f. fasciata*, one leading from *N. f. pictiventris* to *N. c. compressicauda*, and one leading from the base of the tree to *N. c. clarkii* (supplementary fig. S4). At K=7, the best network contained five migration edges, demonstrating the tremendous amount of gene flow occurring within this complex (supplementary fig. S4).

To further identify gene flow and detect potential hybrid origin of populations or subspecies, we used *HyDe* (Blischak et al. 2018) with all possible triples (*i.e.*, parent/hybrid combinations) based on the clusters identified by *DAPC*. We detected evidence of hybrid origin for *N. f. pictiventris*, *N. c. compressicauda*, and *N. c. taeniata* populations with gamma (γ , probability of assignment to one parent) ranging from 0.44 to 0.75 (fig. 4, supplementary S4 & S5). However, populations identified as hybrids also

functioned as parents for other populations (fig. 4, supplementary S4 & S5); therefore, the evolutionary history leading to these populations appears to be a result of rampant hybridization among nearly all populations. Interestingly, *N. c. taeniata* was consistently found to be the result of hybridization between *N. c. clarkii* and *N. f. pictiventris* which may support a previous hypothesis suggesting that *N. c. taeniata* intergrades with neighboring populations and is derived from *N. c. clarkii*, given color pattern similarities (fig. 4, supplementary S4 & S5; Carr and Goin 1942).

To visualize the patterns of gene flow across Florida, we used *EEMS* (Petkova et al. 2016). *EEMS* clearly demonstrates a strong reduction in gene flow between coastal and inland environments and additional weaker reductions along subspecies geographic boundaries (fig. 3B). Specifically, *EEMS* identifies a nearly panmictic inland population, suggesting high gene flow between subspecies of *N. fasciata* (fig. 3B). However, a slight reduction in gene flow can be seen near the Suwanee Straight, consistent with the identification of mainland and peninsular clades in the phylogenetic analyses (fig. 3B, supplementary fig. S3). Similarly, *EEMS* identifies high gene flow among coastal populations and subspecies of *N. clarkii*. A slight barrier may exist between *N. c. clarkii* in northwestern Florida and *N. c. compressicauda*. There is an additional break for *N. clarkii* along the southeast coast of Florida separating eastern and southern clades of *N. c. compressicauda* (fig. 3B). Previously, *N. c. compressicauda* was thought to be absent from southeast Florida coastlines and, due to heavy urbanization, there is little habitat remaining. However, this break may be due to incomplete sampling since *N. c. compressicauda* was recently discovered in this area (Holbrook et al. 2016). Finally, *EEMS* identifies areas of high introgression between *N. fasciata* and *N. clarkii* along both the east and west-central coasts (fig. 3B).

Ecological Niche Divergence

To assess ecological niche divergence between *N. fasciata* and *N. clarkii*, we first used *Humboldt* (Brown and Carnaval 2019) to perform Niche Overlap Tests (NOT) and Niche Divergence Tests (NDT). We downloaded 7,320 occurrence records for *N. fasciata* and *N. clarkii* from the Global Biodiversity Information Facility (1,216 *N. clarkii* and 6,104 *N. fasciata*; GBIF 2019) and removed records outside of Florida and each species distribution resulting in a final dataset of 3,623 records (649 *N. clarkii* and 2,974 *N. fasciata*). The results of *Humboldt* were inconclusive and prone to Type I error due to niche truncation or observations being located close to the edge of the available environmental space, leading to the inability to obtain appropriate background data (supplementary fig. S6; Brown and Carnaval 2019).

Therefore, we further explored the six most informative variables identified by *Humboldt*. These variables primarily included landcover variables such as the amount of regularly flooded vegetation and open water, which was greater in *N. clarkii* (supplementary fig. S6). Notably, however, we found that cation exchange capacity of the soil – a variable highly correlated with salinity (Saidi 2012) – was much higher for *N. clarkii* (supplementary fig. S6). To determine if this pattern was maintained in our genetic clusters,

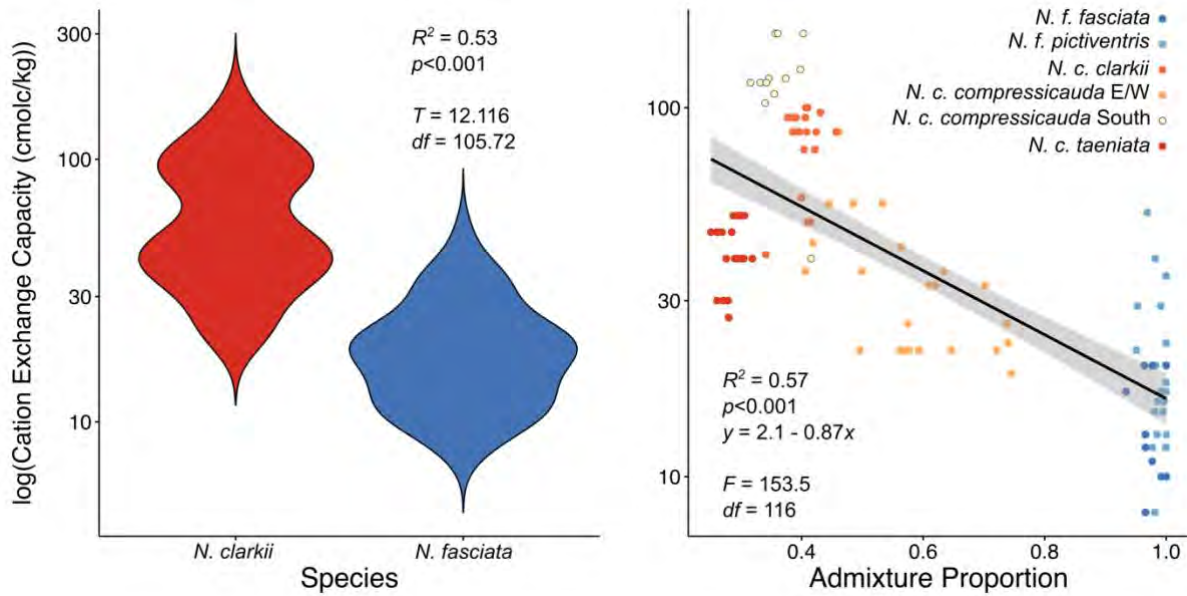


Fig. 5. Violin plot demonstrating the differences in cation exchange capacity of the soil – used as a metric of salinity – between *N. fasciata* and *N. clarkii* based on *DAPC* assignment at $K=2$. Regression of *conStruct* admixture proportion at $K=2$ (proportion assigned to *N. fasciata*) with cation exchange capacity of the soil. Points are colored by *DAPC* assignment at $K=6$.

we extracted cation exchange capacity data for all 118 genetic samples and found significant differences between the two species (*DAPC* $K=2$; $R^2=0.53$; $p < 0.001$; fig. 5). Furthermore, we found a significant relationship with the *conStruct* admixture proportion suggesting that admixture may be limited by salinity ($R^2= 0.57$; $p < 0.001$; fig. 5). However, admixture proportions might represent shared ancestry rather than gene flow. Therefore, to disentangle the influence of IBD and IBE caused by salinity on genetic dissimilarity, we performed a series of Mantel and partial Mantel tests using all individuals and separately for each species (*DAPC* $K=2$). If IBE plays a role in species divergence, we expect a significant correlation when comparing all individuals, but not within each species. Mantel tests confirm that IBD strongly influences our data both across and within a single species ($0.38 \leq r \leq 0.65$; $p = 0.001$). Partial Mantel tests confirm that genetic dissimilarity is associated with differences in salinity when looking across species ($r = 0.15$; $p = 0.001$), but not within *N. fasciata* ($r = -0.30$; $p = 1$) or *N. clarkii* ($r = 0.03$; $p = 0.25$).

Scans for Selection Signatures

Given the ecological differences observed between *N. fasciata* and *N. clarkii*, we sought to identify genes potentially contributing to their divergence. We used *BayeScan* with a reduced dataset, only including *N. clarkii* with $< 50\%$ admixture proportion from *N. fasciata*. *BayeScan* identified 62 outlier SNPs between *N. fasciata* ($n=41$) and *N. clarkii* ($n=60$) which corresponded to 41 loci ($p < 0.05$; supplementary table S3). After searching for genes within 2kb of BLAST matches to the *Thamnophis elegans* reference genome (GCF_009769535.1), we identified 31 potential genes of interest (supplementary table S4). GO-enrichment

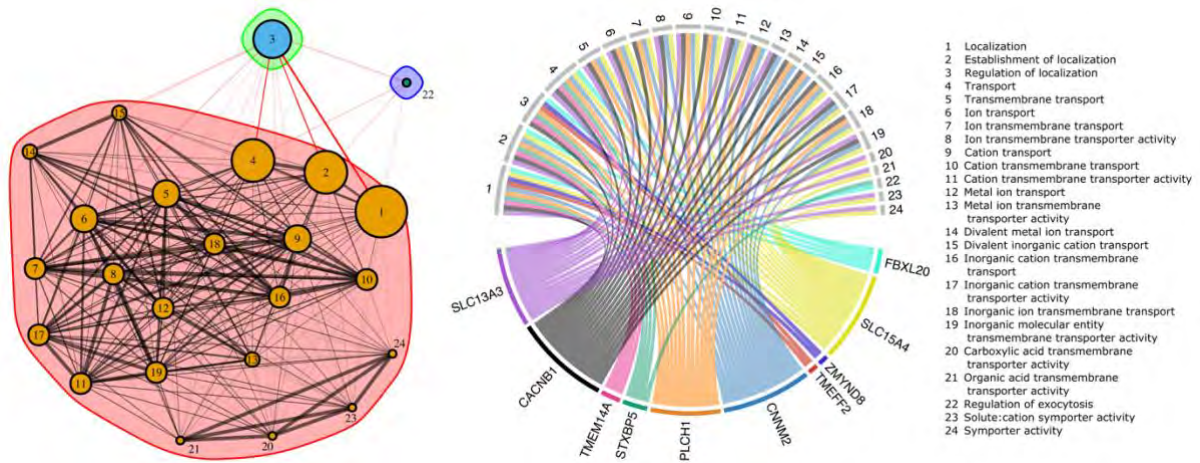


Fig. 6. Left: Network generated by *ShinyGO* of all significantly enriched GO terms for genes shared across *BayeScan* scans. Two nodes are connected if they share greater than 20% of their genes. Node size corresponds to size of the gene sets and edge thickness correspond to the number of overlapped genes. The colored envelopes represent modules with dense nodal connections, but sparse connections to other modules. Right: Genes associated with ion, cation, and transmembrane transport which are likely related to osmoregulatory adaptations associated with coping with saline environments in *N. clarkii*.

analysis identified a network of 24 significantly enriched GO terms (FDR < 0.05) corresponding to 10 genes (fig. 6). The majority of enriched terms are related to transmembrane transport of ions and metals. Specifically, these terms included cation transmembrane transport (GO:0098655), cation transport (GO:0006812), metal ion transport (GO:0030001), and transmembrane transport (GO:0055085; fig. 6). The 10 associated genes likely correspond to changes in osmoregulatory abilities between the two species and the ability to cope with high salinity environments (fig. 6).

Morphology

To evaluate our findings in light of current taxonomy and morphological variation, we measured 11 meristic and dimensional features for 137 specimens across the range (fig. supplementary S8A) and performed principal component analysis. PC1 accounted for 22.7% of the variation and was most influenced by the number of post-ocular scales; PC2 accounted for 16.4% of the variation and was most influenced by the number of subcaudal scales. Model-based clustering in the R package *mclust* (Scrucca et al. 2016) identified two morphological clusters; however, these clusters overlapped heavily in PC space (fig. supplementary S8B). To assess if species or subspecies formed morphological clusters we plotted these variables in PC space (fig. supplementary S8C & S8D) and performed AIC linear model comparison on the first two principal components using the species assignment, subspecies assignment, sex, age, and capture latitude as explanatory variables. We found that species assignment at capture was the best predictor of PC1 (fig. supplementary S9B), but sex was the best predictor of PC2 (fig. supplementary S9C). When only using morphological data with corresponding genetic data ($n = 21$), we found that *conStruct* admixture proportions (K=2) was the best predictor of PC1, demonstrating general agreement between the

morphological and genetic differentiation of *N. fasciata* and *N. clarkii*, with genetically intermediate individuals also having intermediate phenotypes (fig. supplementary S9A). Additionally, using a Mantel test, we found a significant correlation between genetic dissimilarity and morphological distance ($r = 0.24$; $p = 0.01$). However, the amount of morphological difference between species was small and even less between subspecies. The main difference between species is related to the number of post-ocular scales, with a difference of only one scale between the two species.

Discussion

The formation and maintenance of lineages is governed by the homogenizing effects of gene flow and reinforcement of genomic divergence due to ecological and environmental selection (Rundle and Nosil 2005; Yeaman and Whitlock 2011; Tigano and Friesen 2016). We provide compelling evidence that pervasive gene flow and environmental selection, likely caused by differences in salinity, shape the evolutionary history of the *N. fasciata-clarkii* complex. Specifically, we find that IBD explains patterns of population structure, but IBE—caused by differences between inland and coastal habitats and subsequent selection on osmoregulatory genes—better explains broader genetic structure despite introgression from *N. fasciata* into *N. clarkii* and putative hybrid formation of some lineages.

Historic and contemporary gene flow play vital roles in mediating outcomes of incipient speciation, including the establishment of reproductive barriers or, conversely, lineage fusion (Nosil 2008; Tigano and Friesen 2016). Because previous studies have identified hybridization among lineages within the *N. fasciata-clarkii* complex (Conant 1963; Lawson et al. 1991), we expected to find evidence of gene flow among lineages. Our explicit tests of gene flow and population structure analyses find strong evidence of pervasive gene flow and admixture across the *N. fasciata-clarkii* complex. It is well-known that gene flow generates conflicts in phylogenetic signal (Degnan and Rosenberg 2009; Cui et al. 2013; Pease et al. 2016; Mason et al. 2019); therefore, gene flow is likely responsible for the limited nodal support recovered in our phylogenies and further demonstrates the most probable cause of historical phylogenetic discrepancies, with regard to the separation of *N. fasciata* and *N. clarkii*, and limitations of single-gene phylogenies. However, gene flow also played a critical role in the formation of several lineages, particularly *N. c. compressicauda* and *N. c. taeniata*, as demonstrated by *HyDe* (fig. 4). This suggests that gene flow among lineages might, in some cases, facilitate diversification possibly through the introduction of genetic variation. Instances where gene flow and hybridization promote genetic diversity and adaptation by introducing genetic variation are well-documented, including adaptation to high altitudes from Denisovans into humans in Tibet (Huerta-Sánchez et al. 2014; Tigano and Friesen 2016; Patton et al. 2020). Gene flow was widespread among *Nerodia* lineages, but it was asymmetrical. *conStruct* showed that a large proportion of *N. fasciata* alleles were shared with *N. clarkii*, but very few *N. clarkii* alleles were shared with *N. fasciata*

(fig. 3). Although *conStruct* admixture proportions might instead be a result of shared ancestry or differences in effective population size (Lawson et al. 2018), *TreeMix* and *HyDe* analyses similarly indicated that gene flow primarily occurred from *N. fasciata* lineages to *N. clarkii* lineages (fig. 4). Unfortunately, determining the exact nature of the timing and extent of gene flow among these watersnakes requires expanded sampling to include lineages outside the range of Florida as well as explicit tests of alternate demographic histories. Nonetheless, the persistence of *N. clarkii*-specific alleles despite high gene flow suggests selective advantage of these genes.

We found evidence that differential selection based on ecological divergence contributed to the maintenance of genomic divergence between lineages. *Nerodia fasciata* and *N. clarkii* have long been distinguished by putative ecological differences, but we provide empirical evidence of niche differentiation. As hypothesized, cation exchange capacity in the soil—a proxy for salinity—was implicated as an environmental variable potentially limiting admixture and facilitating genetic differentiation of the two species through IBE (fig. 5). These findings are consistent with *EEMS* as the primary barriers to gene flow occur near inland-coastal ecotones where habitat type and salinity may rapidly shift (fig. 3). Salinity might provide a threshold under which admixture can occur, with high-salinity environments having little admixture. However, salinity and admixture are more likely to represent a continuous cline with temporal variation in salinity—which we did not measure—also playing a large role in the degree of admixture between the two species. Further support for the role of salinity driving divergence of these watersnakes was apparent in our scans for signatures of selection, in which the majority of the loci detected as outliers corresponded to genes associated with osmoregulatory function, consistent with previous experimental studies on adaptive responses to salinity stress in plants, fish, and turtles (Zhang et al. 2017; Hong et al. 2019; Mansouri et al. 2019; Lee et al. 2020). For example, we identified two genes from the solute-carrier (SLC) family which have been previously identified in responders to salinity-stress (Zhang et al. 2017; Hong et al. 2019). Unfortunately, establishing causal relationships between our identified candidate genes and increased salt tolerance will require experimental study. Similarly, it would be interesting to investigate the possibility of convergent or parallel evolution of salt tolerance in *N. clarkii* and other salt tolerant reptiles. Nonetheless, strong divergent selection caused by ecological divergence in salinity has likely led to local adaptation and we hypothesize it contributes to divergence in the *N. fasciata-clarkii* complex.

Reconciling the pattern of asymmetric gene flow from *N. fasciata* into *N. clarkii* with the salinity-driven adaptations in *N. clarkii* is counterintuitive since *N. clarkii* are readily found in and invade freshwater habitats and we expect it should be challenging for *N. fasciata* to invade high-salinity environments (although we observed *N. fasciata* in salt marsh habitats). Nonetheless, a similar pattern is seen in Andean Speckled Teals (*Anas flavirostris*) where low-altitude populations migrate at a higher rate into high-altitude populations despite positive selection in hemoglobin genes within high-altitude populations (Graham et al.

2018). The most likely explanation for this pattern is a ‘source-sink’ dynamic between lineages which might reflect the expansion or invasion of the larger and more widely distributed population, *N. fasciata*, into coastal habitats. Following invasion of coastal habitats, selection can favor individuals with adaptations to high-salinity environments leaving the remainder of the genome free to admix (Graham et al. 2018). Future study should focus on estimating the effective population sizes of these two species to elucidate potential ‘source-sink’ dynamics; however, preliminary analysis of nucleotide diversity in these two species supports this hypothesis with significantly higher nucleotide diversity in *N. fasciata* ($\pi = 0.29$) relative to *N. clarkii* ($\pi = 0.25$; $p < 0.001$). An alternate explanation may be exclusion, where *N. clarkii* alleles are less able to permeate into *N. fasciata* due to potential trade-offs with fitness and subsequent inability to compete with the dominant *N. fasciata* populations. Under this scenario, *N. fasciata* likely functions as a generalist capable of moving across the landscape and *N. clarkii* as a coastal specialist.

An ongoing challenge for watersnakes and many other groups with widespread gene flow is reconciling taxonomy with complex, reticulate evolutionary histories. Since the initial description of lineages within the *N. fasciata-clarkii* complex, the nomenclature has undergone frequent revision with lineages being listed as subspecies of the Northern Watersnake (*Nerodia sipedon*), then the Southern Watersnake (*N. fasciata*), and later being re-elevated to species or subspecies based on morphology, allozymes, and ecological differentiation (Carr and Goin 1942; Lawson et al. 1991; reviewed in Territo 2013). While we confirm ecological divergence of *N. fasciata* and *N. clarkii* in Florida and document evidence indicative of local adaptation, we also show a clear lack of reproductive isolation and no clear trend of morphological variation corresponding to recognized taxonomy. Therefore, our data are inconclusive with regard to taxonomy and only support that the *N. fasciata-clarkii* complex represent a case of incipient speciation, falling within the speciation continuum which may eventually diverge or coalesce (De Queiroz 2007). An alternative but complementary interpretation of our results is that this complex represents a single species with local adaptation along the coasts; however, without additional sampling from across the range of the *N. fasciata-clarkii* complex and explicit delimitation of species including demography and timing of divergence, we choose to avoid premature nomenclatural changes (Hillis 2019; Hillis 2020). Specifically, the timing of gene flow among our populations is uncertain and the observed patterns of admixture and gene flow could be consistent with allopatry followed by secondary contact or by ongoing divergence with gene flow. Additional genomic data, sampling from across the range of the *N. fasciata-clarkii* complex, and fine-scale analyses are required to better understand the intraspecific structure and adequately assess taxonomy. Notably, however, the federally-listed subspecies, *N. c. taeniata*, may have the lowest proportion of admixture of the *N. clarkii* subspecies, suggesting further work be done to evaluate the evolutionary distinctiveness of this lineage. Together, with the results on ecological divergence, our results suggest that isolation-by-distance explains subspecies or population structure, similar to what was previously found for

N. c. compressicauda by Jansen et al. (2008). However, isolation-by-environment likely explains species divergence with genomic regions resistant to gene flow and locally adapted to high-salinity environments. The *N. fasciata-clarkii* complex is but one of many representative groups which rejects the bifurcating speciation model in favor of a more reticulate pattern (Choi et al. 2019; Dean et al. 2019; Edelman et al. 2019; Mason et al. 2019). As studies documenting gene flow and reticulate evolution (even among established species) increase in frequency, it is critical to consider how to best address taxonomy and ultimately conservation.

Phylogenomics and novel methodologies testing for violations of the bifurcating tree model have allowed gene flow and reticulate evolution to be widely recognized as a common process in lineage diversification (Nosil 2008; Barth et al. 2020). Given these technological developments, evolutionary biologists are able to more easily identify the forces and processes underlying incipient speciation with gene flow and begin to reconcile this with taxonomy and nomenclature. Environmental divergence can facilitate selection for local adaptation creating regions in the genome resistant to gene flow, but leaving the remainder of the genome free to admix. This pattern of divergent genomic islands follows a model of genetic hitchhiking (Feder et al. 2012). However, if divergence does not continue and the migration-selection balance is stable, reconciling the high degree of admixture with taxonomy has considerable implications, particularly for conservation. Consequently, it is critical to identify the mechanisms and regions of the genome underlying lineage divergence and explore alternate evolutionary histories, including reticulate evolution, to understand the speciation process.

Methods

Sampling

We sampled *Nerodia fasciata* and *N. clarkii*, including all subspecies, from throughout Florida; we attempted to encompass individuals and localities from each potential habitat. Snakes were captured via road cruising or surveys in suitable habitat throughout Florida. Upon capture, locality was recorded and tissue was either taken in the field – via tail-tips, scale-clips, or blood draws – or the specimen was processed, vouchered, and deposited following AVMA guidelines (Leary et al. 2013). Species and subspecies identity were recorded for each sample using a combination of geography and preliminary morphological examination, according to the original subspecies descriptions (Baird and Girard 1853; Kennicott 1860; Cope 1895). If identity was uncertain, samples were recorded as such; however, all analyses were performed using unbiased clustering methods. Specimens were deposited at the Florida Museum of Natural History under accessions given in supplementary table S1. Snakes were handled and collected under the following permits and Animal Care and Use Protocols: University of Central Florida IACUC (09-28W, 11-41W, 14-26W, and 15-39W), Florida Fish and Wildlife Conservation Commission

(LSV-09-0295), Florida Department of Environmental Protection Division of Recreation and Parks (#8261020) and the United States Fish and Wildlife Service (TE220923-D).

Sanger Sequencing

To determine phylogenetic structure, we first amplified and sequenced the cytochrome b gene (*cytb*: Burbrink et al. 2000) for 268 individuals and 20 outgroups (supplementary table S1). We then selected a subset of 85 individuals and 11 outgroup taxa for additional gene sequencing and analyses (supplementary table S1). In addition to *cytb* for these individuals, we amplified and sequenced NADH dehydrogenase subunits 1 (*ND1*: Jiang et al. 2007) and 4 (*ND4*: Arevalo et al. 1994), the nuclear gene Prolactin Receptor (*PRLR*: Townsend et al. 2008), the anonymous loci *M* and *E* (Mcvay et al. 2015), and the nuclear intron *TATA* (Wood et al. 2011). DNA was extracted from tissue samples using either a Qiagen DNeasy Kit or Serapure beads following the procedure from Faircloth and Glenn (2014). Genes were amplified using standard polymerase chain reaction (PCR) following the referenced studies or were optimized for samples where there was no initial amplification. All sequences were generated using Sanger sequencing by either the University of Arizona Genetics Core or Eurofins Genomics.

We aligned genes using *MUSCLE* (Edgar 2004) and manually inspected. We generated gene trees for each locus and also carried out phylogenetic analyses on three concatenated datasets: 1) an alignment of all loci, 2) an alignment of mitochondrial loci, and 3) an alignment of nuclear loci. We generated maximum-likelihood and Bayesian inference phylogenetic trees using *RAxML* v.8.2.12 (Stamatakis 2014) and *MrBayes* v.3.2.7 (Ronquist et al. 2012), respectively. In all analyses, protein coding loci were partitioned by codon position and models of substitution were determined with *PartitionFinder* v. 2.1.1 (Lanfear et al. 2016). See supplementary table S2 for alignment partitions and models. *RAxML* trees were generated with 20 independent searches with the substitution models set to GTR-GAMMA for all alignments. We annotated the resulting best tree with nodal support values attained by performing 1,000 bootstrap replicates. *MrBayes* analyses were run two independent times with one cold and three heated chains. Priors were set to program defaults with a variable rate prior across partitions. Chains were run for 10 million generations, sampling every 1,000 generations and the first 10% of samples were discarded as burnin. Stationarity of the chain was evaluated using *Tracer* (Rambaut et al. 2018). All trees were viewed in *FigTree*.

ddRAD-Seq

We extracted DNA from blood, liver, or scale tissue using a standard phenol-chloroform extraction on 131 snakes. These individuals were chosen to encompass the variation observed within these taxa and individuals representing each of the described species/subspecies. We used a Qubit Fluorometer 3 (Thermo Fisher Scientific, Waltham, MA, USA) to quantify extractions, requiring 500-1000 ng of DNA for ddRADseq. Our ddRADseq protocol follows Peterson et al. (2012) with some modifications. Briefly, we

digested DNA for a minimum of 8 hours at 37°C using the rare cutting restriction enzyme SbfI-HF (8 bp) and the common cutting restriction enzyme Sau3AI (4 bp). We purified samples using AMPure magnetic beads (Beckman Coulter, Inc., Irving, TX, USA) at a 1.1:1 bead-to-DNA ratio and eluted in 42uL of tris-HCl (pH 8.0) for quantification. Based on DNA concentration, we divided samples into groups of eight samples. To ensure similar coverage across samples, each group was assigned a standardized amount of DNA based on the lowest DNA concentration per group before ligation. One of 16 double-stranded DNA adaptors, or inline barcodes, was ligated to the end of the digested DNA fragments from each individual. These barcodes are necessary for sample identification after sequencing. Barcodes were ligated at 16°C for 5 hours. After ligation we cleaned each sample using AMPure beads at a 1.1:1 bead-to-DNA ratio and quantified DNA using Qubit. If necessary, samples were rearranged into new groups to minimize differences in DNA concentration. We pooled and cleaned groups with AMPure magnetic beads and eluted with 30uL of TE (pH 8.0). We used a Pippin Prep (Sage Science) with a 1.5% agarose gel to size select fragments from 300–700 bp in length. This size-range was selected to recover the maximum number of potential loci for downstream analyses (Schield et al. 2015). The DNA fragments in each group were amplified using PCR following Schield et al. (2015). Each group was assigned a unique primer that adds a second index barcode to each sample during the PCR. This results in 128 unique barcode-index combinations. We cleaned samples twice at a 0.7:1 bead ratio and quantified on the Qubit. We confirmed concentration and library quality using a high-sensitivity DNA chip for the BioAnalyzer 2100 (Agilent Genomics) which confirm the appropriately sized fragments were amplified. We sequenced our libraries on an Illumina Nextseq 550 using 150 bp paired-end reads.

Variant Calling

We used the *ipyrad* v0.7.28 (Eaton 2014; Eaton and Overcast 2020) toolkit to demultiplex reads, assemble loci, and call SNPs, with default parameters, unless otherwise specified. Briefly, each library had the first 8 base pairs trimmed using *Trimmomatic* v0.38 (Bolger et al. 2014) prior to demultiplexing to remove adapter/primer sequence. After demultiplexing, low quality sites ($Q < 20$) were trimmed from the 3' end of reads or changed to ambiguities (N). Reads with more than five ambiguities or that were less than 100 bp were removed. Reads were then clustered *de novo* within individuals using a 90% similarity threshold. Next, consensus allele sequences were estimated, considering an estimated sequencing error rate (0.003) and heterozygosity (0.02) across all sites. Only sites between 6–10,000x coverage and reads with less than 5 uncalled bases were used for genotyping. Using the same similarity threshold, consensus sequences were clustered across individuals and then aligned. Loci with more than eight heterozygous sites, or which occurred in less than 4 individuals, were removed.

We used *VCFtools* v0.1.15 (Danecek et al. 2011) to further filter SNPs. Individuals were removed if they had fewer than 1000 loci. Next, in order to ensure high quality SNPs, we removed any non-biallelic

SNPs as well as SNPs that had more than 50% missing data, a mean depth of less than 10x across individuals, and minor allele frequency greater than 5%. The `-depth` flag was used to find the mean depth of each individual across all their reads and individuals below 5x were removed in order to remove individuals with low quality data. This resulted in a final dataset of 119 individuals (including the outgroup) with 2,260 loci containing 7,057 SNPs.

Population Structure & Phylogenomics

First, we used a discriminant analysis of principal components, or *DAPC* (Jombart et al. 2010), in the *adegenet* package in R (R Core Team 2020) to identify distinct genetic clusters. The best number of clusters was identified with *k*-means clustering and models compared with Bayesian Information Criterion (BIC) for $K = 1-20$ with all principal components retained (supplementary fig. S2). Models with a $\Delta\text{BIC} < 2$ were considered the best number of clusters. We then used *DAPC* to describe the clusters with the number of principal component axes retained chosen via cross-validation using 100 replicates and a training proportion of 0.9.

Additionally, we tested for population structure using the R package *conStruct* to dissociate population structure from continuous clines of genetic variation (Bradburd et al. 2018). First, *vcf* files were converted to *Structure* input files using *plink* (Chang et al. 2015) and a pairwise distance matrix among samples was generated. To test if spatially-aware models were better fit than nonspatial models, we performed cross validation for $K = 1-7$ with 10 replicates per value of K , 100,000 iterations per replicate, and a training proportion of 0.9. Cross-validation demonstrated that spatially aware models always performed better and suggested isolation-by-distance is a feature of our data (supplementary fig. S3). However, in the cross-validation analysis, we found strong support for each increasing value of K . Therefore, to assess how much each additional layer (K) contributes to the explanation of the data, we also performed an analysis of layer contributions. Specifically, we ran a spatially-aware construct analysis for $K = 2-7$ with 3 MCMC chains and 10,000 iterations per MCMC. Layer contributions from each model were then loaded and plotted (supplementary fig. S4).

To infer a phylogeny from the SNP data, we ran *SVDquartets* (Chifman and Kubatko 2014) with a random sample of 500,000 quartets, 1,000 bootstrap replicates, and *Thamnophis saurita* set as the outgroup. Specifically, we converted SNPs to a nexus alignment with two alleles per individual. Lineage and species trees were inferred by partitioning based on the individuals (coalescing alleles from the same individual together) and the *DAPC* clusters, respectively. A majority rule consensus tree was inferred from the bootstrap replicates.

Gene Flow

To test for evidence of gene flow among populations, we ran *Treemix* (Pickrell and Pritchard 2012) on the *DAPC* identified populations at $K=5, 6,$ and 7 . Based on the results from *SVDquartets*, we rooted *Treemix*

with the *N. f. fasciata* population and allowed 0–15 migration events with 10 iterations per migration edge. To account for linkage disequilibrium and provide confidence in the population graph, we used bootstrap resampling in blocks of 1,000 SNPs (-k 1000). To estimate the optimal number of migration edges for each value of K, we used the R package *OptM* (Fitak 2020) using the default Evanno method. The number of migration edges was chosen based on a plateau of log likelihood and when greater than 99.8% of the variance was explained.

In addition, we used the program *HyDe* (Blischak et al. 2018) to detect hybrids and gene flow. Specifically, *HyDe* uses phylogenetic invariants arising under a coalescent model with hybridization. We ran *HyDe* using all possible combinations of triples (*i.e.*, parent-hybrid relationships) based on the *DAPC* clusters at K=5, 6, and 7. We then ran 200 bootstrap replicates on the significant *HyDe* results and plotted the resulting bootstrap values of gamma (γ) using *ggplot2* (Wickham 2016) and *ggridges* (Wilke 2020).

To determine if the direction of gene flow might be due to differences in effective population size, we calculated nucleotide diversity (π) for each species (*DAPC* K=2) as an indicator of effective population size. Nucleotide diversity was calculated in *VCFtools* and compared using a t-test in R.

To visualize inferred migration rates in the *N. fasciata-clarkii* complex in geographic space, we used the program *EEMS* (Petkova et al. 2016). *EEMS* estimates effective migration by visualizing regions where genetic dissimilarity decays quickly. It relates effective migration rates to expected genetic dissimilarities to define spatial features of population structure across the landscape. We estimated gene flow with *EEMS* across Florida by running 3 independent chains, each with 1,000 demes, for 2,000,000 MCMC iterations, with 500,000 iterations of burn-in and a thinning interval of 1,000. We plotted the results to check for agreement across all three chains and checked for MCMC convergence using the R package, *rEEMSplots*. After failing to converge, we restarted each chain for another 1,000,000 MCMC iterations with 0 burn-in after which the chains converged.

Ecological Niche Divergence

To assess ecological niche divergence between *N. fasciata* and *N. clarkii*, we downloaded 7,320 occurrence records from GBIF (1,216 *N. clarkii* and 6,104 *N. fasciata*; GBIF 2019). Records outside of Florida were removed and further cleaned by removing points outside of the distribution for each species obtained from IUCN resulting in a final dataset of 3,623 records (649 *N. clarkii* and 2,974 *N. fasciata*). For the input environmental data, we used the BioClim dataset from the WorldClim database with spatial resolution of 30 arcsec (Hijmans et al. 2005), cation exchange capacity and pH of soils from the SoilGrid database at a depth of 5 cm and with a spatial resolution of 30 arcsec (Hengl et al. 2017), and landcover data from the EarthEnv database with a spatial resolution of 30 arcsec (Tuanmu and Jetz 2014). Importantly, cation exchange capacity of soil is highly correlated with salinity and used as a proxy for salinity (Saidi 2012). Environmental variables were reduced to only variables which contributed greater than 5% to the model

for either species. Next, we used *Humboldt* to perform Niche Overlap Test (NOT) and Niche Divergence Test (NDT) using corrected e-space across the full distribution and shared e-space, respectively (Brown and Carnaval 2019). *Humboldt* found a nonsignificant equivalency statistic ($p > 0.05$) for both the NOT and NDT and mixed significance for the background statistics (supplementary fig. S6). These results suggest that the niches between these two species might be equivalent (Schoener's $D = 0.37$); however, the tests are inconclusive and prone to Type I error (supplementary fig. S6). To further explore this, we calculated the potential niche truncation index (PNTI; Brown and Carnaval 2019) and found high potential niche truncation for *N. fasciata* (PNTI > 0.73). In other words, because *N. fasciata* occupies nearly all of Florida and *N. clarkii* is near the edge of available environmental space (*i.e.*, coastal habitats), *Humboldt* is unable to sample appropriate background data to provide conclusive results.

To circumvent these issues, we looked for differences in the most important environmental variables identified by *Humboldt* for both GBIF data and assigned genetic clusters by extracting environmental data for each point and comparing species with *ggpubr* (Kassambara 2019). In addition, we performed linear regression of *conStruct* admixture proportion (*i.e.*, proportion assigned to *N. fasciata*) and cation exchange capacity using *ggpubr*. Finally, we performed Mantel and partial Mantel tests to disentangle the influence of IBD and IBE caused by salinity. Specifically, we tested for correlations between genetic dissimilarity (as calculated for *EEMS*), geographic distance (km), and environmental distance (calculated as the Euclidian distance between each samples value for cation exchange capacity). To test for IBD, we performed a Mantel test between genetic dissimilarity and geographic distance. To test for IBE, we performed a partial Mantel test between genetic dissimilarity and environmental distance, controlling for geographic distance. These tests were performed on three datasets: (1) all individuals, (2) *N. fasciata* only (*DAPC* $K=2$), and (3) *N. clarkii* only (*DAPC* $K=2$).

Scans for Selection Signatures

To test for signatures of selection between *N. fasciata* and *N. clarkii*, we searched for outlier SNPs using *BayeScan* (Foll and Gaggiotti 2008), blasted outlier loci to a reference genome to identify nearby genes, and identified enriched gene ontology (GO) terms. First, we subset our data to only include *N. clarkii* individuals with $< 50\%$ admixture with *N. fasciata*. Our final dataset included 101 individuals (60 *N. clarkii*, and 41 *N. fasciata*). The resulting data were converted to *BayeScan* format with *PGDSpider* (Lischer and Excoffier 2012). We ran *BayeScan* using default settings (*i.e.*, 5000 output iterations, 20 pilot runs, pilot run length of 5000, 50000 iterations of burn-in, and a thinning interval of 10). The loci with SNPs that were identified as significant ($p < 0.05$; $n = 62$ SNPs & 41 loci; supplementary table S3) were blasted against the *Thamnophis elegans* genome (GCF_009769535.1) using *blastn* returning a maximum of five hits and hsp with a stringent e-value of $1e-50$ (supplementary table S4). We converted BLAST hits to a bed file (<https://github.com/nterhoeven/blast2bed>) and genes that were within 2,000 bp of a hit within the genome

were extracted as potential genes of interest. To search for enriched GO terms, we used *ShinyGO* (Ge et al. 2019) using the *Gallus gallus* genome, a FDR cutoff of 0.05, and extracting the 30 most significant terms. We chose to use the chicken genome as our GO reference because it is the most closely related and complete database. Other reptilian databases (e.g., Anole) are less complete and do not have functional information matching many of the identified genes. We used the R package *igraph* (Csárdi and Nepusz 2006) to plot networks and identify modules with dense connections (`cluster_edge_betweenness`). Finally, we used the R package *circlize* (Gu et al. 2014) to plot connections of genes and enriched GO terms.

Morphology

We counted or measured a total of 11 meristic and dimensional features for 137 specimens representing 24 *Nerodia clarkii* (8 *N. c. clarkii*, 7 *N. c. compressicauda*, and 9 *N. c. taeniata*), 95 *N. fasciata* (21 *N. f. fasciata*, 71 *N. f. pictiventris*), and 21 with uncertain assignment to a taxon. Of the 11 features, we measured several diagnostic characters including the number of ventral scales, subcaudal scales, and tail length (Carr and Goin 1942). We measured snout-vent length (SVL) to standardize tail length and also counted mid-body scale row. Lastly, we counted the number of supralabial scales, infralabial scales, and post-ocular scales on the left and right side of the body independently. To visualize morphological variation, we performed principal component analysis (PCA) with 95% confidence ellipses in R with the packages *ggpubr*. We used the first two principal component axes to perform model-based clustering analysis to identify the most likely clusters using the R package *mclust* (Scrucca et al. 2016). To determine what factors best explain the differences in PC1 and PC2, we created a set of linear models in R (R Core Team 2020) using the species assignment, subspecies assignment, sex, age, and capture latitude as explanatory variables and compared the models using AIC with the package *bbmle* (Bolker and R Development Core Team 2019). Species and subspecies assignment were based on the assignment at capture ($n = 137$) and when only using samples with corresponding genetic data ($n = 21$) we used *DAPC* assignment and *conStruct* admixture proportion to assess agreement between morphological and genetic datasets. We also performed a Mantel test between genetic dissimilarity (as calculated for *EEMS*) and the Euclidian distance of PC1.

Data Availability

The data underlying this article are available in its online supplementary material and the National Center for Biotechnology Information (NCBI). ddRAD-Seq data were submitted to the Sequence Read Archive (SRA) under BioProject (PRJNA646486). BioSample (SAMN15544064 – SAMN15544182) and SRA (SRR12229022 – SRR12229140) accession numbers can be found in supplementary table S1. Accession numbers for *cytb*, *ND1*, *ND4*, *PRLR*, *M*, *E*, *TATA* (MT801183 – MT801894) can also be found in supplementary table S1. Morphological data are provided in supplementary table S1. Ecological data was obtained from publicly available databases and all analytical softwares are publicly available.

Acknowledgments

We thank Billy Brooks (USFWS), Kevin Enge (Florida Fish and Wildlife Conservation Commission - FWC), Paul Moler (FWC), Donna Watkins (Florida Department of Environmental Protection-DEP), Graham Williams (Florida DEP), and Alice Bard (Florida DEP) for their assistance with permitting, sampling, and general guidance. Funding for this research was provided by the USFWS and the FWC via section 6 monies. For computational resources and suggestions, we thank the Clemson University Genomics and Bioinformatics Facility (CUGBF) which is partially supported by an Institutional Development Award (IDeA) from the National Institute of General Medical Sciences of the National Institutes of Health: P20GM109094 and Clemson University for providing additional computational resources on the Palmetto HP cluster. For specimen and tissue donations, we thank the Florida Museum of Natural History, Kevin Enge, Paul Moler, Ken Sims, Pierson Hill, Kenny Wray, and Jim Peters. We thank Mathew Tragash, Joshua Castro, Jimi Cheak, Josh Holbrook, Ed Metzger, Alex Robertson, Ramin Beheshti, Robbie McKenna, Bridget Vincent, Katelyn Lanctot, and Carly Grimison for helping with sampling, morphometrics, and/or genetic lab work. We thank Eric Hoffman, John Fauth, Michelle Gaynor, Erich Hofmann, and Erin Stiers for providing assistance, guidance, and/or advice to improve this study. We thank Coleman Sheehy and David Blackburn of the Florida Museum of Natural History for help in specimen deposition and cataloging. Finally, we thank Gregory Territo and Jason Hickson for help in all aspects of this paper including sampling, morphometrics, genetics, and providing invaluable comments which improved this manuscript.

References

- Arévalo E, Davis SK, Sites Jr. JW. 1994. Mitochondrial DNA Sequence Divergence and Phylogenetic Relationships among Eight Chromosome Races of the *Sceloporus grammicus* Complex (Phrynosomatidae) in Central Mexico.
- Babonis LS, Miller SN, Evans DH. 2011. Renal responses to salinity change in snakes with and without salt glands. *J. Exp. Biol.* 214:2140–2156.
- Baird SF, Girard C. 1853. Catalogue of North American Reptiles in the Museum of the Smithsonian Institution. Part 1. Serpents. Washington DC, USA
- Barth JMI, Gubili C, Matschiner M, Tørresen OK, Watanabe S, Egger B, Han Y, Feunteun E, Sommaruga R, Jehle R, et al. 2020. Stable species boundaries despite ten million years of hybridization in tropical eels. *Nat. Commun.* 11:1433.
- Blischak PD, Chifman J, Wolfe AD, Kubatko LS. 2018. HyDe: A python package for genome-scale hybridization detection. *Syst. Biol.* 67:821–829.

- Bolger AM, Lohse M, Usadel B. 2014. Trimmomatic: A flexible trimmer for Illumina sequence data. *Bioinformatics* 30:2114–2120.
- Bolker B, R Development Core Team. 2019. bbmle: Tools for General Maximum Likelihood Estimation. Available from: <https://cran.r-project.org/package=bbmle>
- Bradburd GS, Coop GM, Ralph PL. 2018. Inferring continuous and discrete population genetic structure across space. *Genetics* 210:33–52.
- Brown JL, Carnaval AC. 2019. A tale of two niches: methods, concepts and evolution. *Front. Biogeogr.* 11.
- Burbrink FT, Lawson R, Slowinski JB. 2000. Mitochondrial DNA phylogeography of the polytypic North American rat snake (*Elaphe obsoleta*): A critique of the subspecies concept. *Evolution* (N. Y). 54:2107–2118.
- Campbell CR, Poelstra JW, Yoder AD. 2018. What is Speciation Genomics? The roles of ecology, gene flow, and genomic architecture in the formation of species. *Biol. J. Linn. Soc.* 124:561–583.
- Carr AFJ, Goin CJ. 1942. Rehabilitation of *Natrix sipedon taeniata* Cope. *Proc. New Engl. Zool. Club* 21:47–54.
- Chang CC, Chow CC, Tellier LCAM, Vattikuti S, Purcell SM, Lee JJ. 2015. Second-generation PLINK: Rising to the challenge of larger and richer datasets. *Gigascience* 4:1–16.
- Chifman J, Kubatko L. 2014. Quartet inference from SNP data under the coalescent model. *Bioinformatics* 30:3317–3324.
- Choi JY, Purugganan M, Stacy EA. 2019. Divergent selection and primary gene flow shape incipient speciation of a riparian tree on Hawaii Island. *Mol. Biol. Evol.* 37:695–710.
- Conant R. 1963. Evidence for the specific status of the water snake *Natrix fasciata*. *Am. Museum Novit.* 2122:1–38.
- Cope ED. 1895. On some North American Snakes. *Am. Nat.* 29:676–680.
- Csárdi G, Nepusz T. 2006. The igraph software package for complex network research. *InterJournal [Internet] Complex Sy.* Available from: <http://igraph.org>
- Cui R, Schumer M, Kruesi K, Walter R, Andolfatto P, Rosenthal GG. 2013. Phylogenomics Reveals Extensive Reticulate Evolution In Xiphophorus Fishes. *Evolution* (N. Y). 67:2166–2179.
- Danecek P, Auton A, Abecasis G, Albers CA, Banks E, DePristo MA, Handsaker RE, Lunter G, Marth GT, Sherry ST, et al. 2011. The variant call format and VCFtools. *Bioinformatics* 27:2156–2158.
- Dean LL, Magalhaes IS, Foote A, D'Agostino D, McGowan S, MacColl ADC. 2019. Admixture between Ancient Lineages, Selection, and the Formation of Sympatric Stickleback Species-Pairs. *Mol. Biol. Evol.* 36:2481–2497.
- Degnan JH, Rosenberg NA. 2009. Gene tree discordance, phylogenetic inference and the multispecies

- coalescent. *Trends Ecol. Evol.* 24:332–340.
- Dunson WA. 1980. The Relation of Sodium and Water Balance to Survival in Sea Water of Estuarine and Freshwater Races of the Snakes *Nerodia fasciata*, *N. sipedon* and *N. valida*. *Copeia* 1980:268–280.
- Eaton DAR. 2014. PyRAD: Assembly of de novo RADseq loci for phylogenetic analyses. *Bioinformatics* 30:1844–1849.
- Eaton DAR, Overcast I. 2020. ipyrad: Interactive assembly and analysis of RADseq datasets. *Bioinformatics*:2–4.
- Edelman NB, Frandsen PB, Miyagi M, Clavijo B, Davey J, Dikow RB, García-Accinelli G, Van Belleghem SM, Patterson N, Neafsey DE, et al. 2019. Genomic architecture and introgression shape a butterfly radiation. *Science* (80-.). 366:594–599.
- Edgar RC. 2004. MUSCLE: Multiple sequence alignment with high accuracy and high throughput. *Nucleic Acids Res.* 32:1792–1797.
- Endler JA. 1977. Geographic variation, speciation, and clines. *Monogr. Popul. Biol.*
- Faircloth BC, Glenn TC. 2014. Protocol: Preparation of an AMPure XP substitute (AKA Serapure). Web document doi: 10.6079/J9MW2F26.
- Feder JL, Egan SP, Nosil P. 2012. The genomics of speciation-with-gene-flow. *Trends Genet.* 28:342–350.
- Fitak RR. 2020. optM: an R package to optimize the number of migration edges using threshold models (Submitted). *J. Hered.*
- Foll M, Gaggiotti O. 2008. A genome-scan method to identify selected loci appropriate for both dominant and codominant markers: A Bayesian perspective. *Genetics* 180:977–993.
- Garant D, Forde SE, Hendry AP. 2007. The multifarious effects of dispersal and gene flow on contemporary adaptation. *Funct. Ecol.* 21:434–443.
- Garcia-Ramos G, Kirkpatrick M. 1997. Genetic Models of Adaptation and Gene Flow in Peripheral Populations. *Evolution* (N. Y). 51:21.
- GBIF.org (5 December 2019) GBIF Occurrence Download <https://doi.org/10.15468/dl.5isrrp>
- Ge SX, Jung D, Yao R. 2019. ShinyGO: a graphical gene-set enrichment tool for animals and plants. *Bioinformatics*:1–2.
- Gibbons JW, Dorcas ME. 2004. North American Watersnakes: A Natural History. University of Oklahoma Press
- Graham AM, Lavretsky P, Muñoz-Fuentes V, Green AJ, Wilson RE, McCracken KG. 2018. Migration-selection balance drives genetic differentiation in genes associated with high-altitude function in the speckled teal (*Anas flavirostris*) in the andes. *Genome Biol. Evol.* 10:14–32.

- Gu Z, Gu L, Eils R, Schlesner M, Brors B. 2014. *circlize* implements and enhances circular visualization in R. *Bioinformatics* 30:2811–2812.
- Haldane JBS. 1930. A mathematical theory of natural and artificial selection. (Part VI, Isolation.). *Math. Proc. Cambridge Philos. Soc.*
- Hengl T, De Jesus JM, Heuvelink GBM, Gonzalez MR, Kilibarda M, Blagotić A, Shangguan W, Wright MN, Geng X, Bauer-Marschallinger B, et al. 2017. SoilGrids250m: Global gridded soil information based on machine learning. *PLoS One* 12:1–40.
- Hijmans RJ, Cameron SE, Parra JL, Jones PG, Jarvis A. 2005. Very high resolution interpolated climate surfaces for global land areas. *Int. J. Climatol.* 25:1965–1978.
- Hillis DM. 2019. Species Delimitation in Herpetology. *J. Herpetol.* 53:3.
- Hillis DM. 2020. The Detection and Naming of Geographic Variation Within Species. *Herpetol. Rev.* 51:52–56.
- Holbrook JD, Chesnes T, Boss H, Berman A, Chiyka J, Bell Christopher, Bell Caleb. 2016. *Nerodia clarkii compressicauda* (Mangrove Saltmarsh Watersnake). USA: FLORIDA: Martin Co. *Herpetol. Rev.* 47:84.
- Hong M, Jiang A, Li N, Li W, Shi H, Storey KB, Ding L. 2019. Comparative analysis of the liver transcriptome in the red-eared slider *Trachemys scripta elegans* under chronic salinity stress. *PeerJ* 2019:1–19.
- Huerta-Sánchez E, Jin X, Asan, Bianba Z, Peter BM, Vinckenbosch N, Liang Y, Yi X, He M, Somel M, et al. 2014. Altitude adaptation in Tibetans caused by introgression of Denisovan-like DNA. *Nature* 512:194–197.
- Ingvarsson PK. 2001. Restoration of genetic variation lost – the genetic rescue hypothesis. *Trends Ecol. Evol.* 16:62–63.
- Jansen KP. 2001. Ecological genetics of the Salt Marsh Snake *Nerodia clarkii*.
- Jansen KP, Mushinsky HR, Karl SA. 2008. Population genetics of the mangrove salt marsh snake, *Nerodia clarkii compressicauda*, in a linear, fragmented habitat. *Conserv. Genet.* 9:401–410.
- Jiang ZJ, Castoe TA, Austin CC, Burbrink FT, Herron MD, McGuire JA, Parkinson CL, Pollock DD. 2007. Comparative mitochondrial genomics of snakes: Extraordinary substitution rate dynamics and functionality of the duplicate control region. *BMC Evol. Biol.* 7.
- Jombart T, Devillard S, Balloux F. 2010. Discriminant analysis of principal components: a new method for the analysis of genetically structured populations. *BMC Genet.* 11:94.
- Kassambara L. 2019. ggpubr: “ggplot2” Based Publication Ready Plots. Available from: <https://cran.r-project.org/package=ggpubr>
- Kennicott R. 1860. Descriptions of new species of North American serpents in the museum of the

- Smithsonian Institution. Proc. Acad. Nat. Sci. Philadelphia. 12:328–338.
- Lamichhaney S, Berglund J, Almén MS, Maqbool K, Grabherr M, Martinez-Barrio A, Promerová M, Rubin CJ, Wang C, Zamani N, et al. 2015. Evolution of Darwin’s finches and their beaks revealed by genome sequencing. *Nature* 518:371–375.
- Lanfear R, Frandsen PB, Wright AM, Senfeld T, Calcott B. 2016. PartitionFinder 2: new methods for selecting partitioned models of evolution for molecular and morphological phylogenetic analyses. *Mol. Biol. Evol.* 34:772–773.
- Lawson DJ, van Dorp L, Falush D. 2018. A tutorial on how not to over-interpret STRUCTURE and ADMIXTURE bar plots. *Nat. Commun.* 9:1–11.
- Lawson R, Meier AJ, Frank PG, Moler PE, Lawson R, Meier AJ, Frank PG. 1991. Allozyme Variation and Systematics of the *Nerodia fasciata-Nerodia clarkii* Complex of Water Snakes (Serpentes : Colubridae). *Copeia* 1991:638–659.
- Leary S, Underwood W, Anthony R, Cartner S, Corey D, Grandin T, Greenacre C, McCrackin MA, Meyer R, Miller D, et al. 2013. *AVMA Guidelines for the Euthanasia of Animals: 2013 Edition*.
- Lee SY, Lee HJ, Kim YK. 2020. Comparative transcriptome profiling of selected osmotic regulatory proteins in the gill during seawater acclimation of chum salmon (*Oncorhynchus keta*) fry. *Sci. Rep.* 10:1–14.
- Lenormand T. 2002. Gene flow and the limits to natural selection. *Trends Ecol. Evol.* 17:183–189.
- Lischer HEL, Excoffier L. 2012. PGDSpider: An automated data conversion tool for connecting population genetics and genomics programs. *Bioinformatics* 28:298–299.
- Mansouri M, Naghavi MR, Alizadeh H, Mohammadi-Nejad G, Mousavi SA, Salekdeh GH, Tada Y. 2019. Transcriptomic analysis of *Aegilops tauschii* during long-term salinity stress. *Funct. Integr. Genomics* 19:13–28.
- Margres MJ, Patton A, Wray KP, Hassinger ATB, Ward MJ, Lemmon EM, Lemmon AR, Rokyta DR. 2019. Tipping the scales: The migration–selection balance leans toward selection in snake venoms. Wray G, editor. *Mol. Biol. Evol.* 36:271–282.
- Mason AJ, Grazziotin FG, Zaher H, Lemmon AR, Moriarty Lemmon E, Parkinson CL. 2019. Reticulate evolution in nuclear Middle America causes discordance in the phylogeny of palm-pitvipers (Viperidae: *Bothriechis*). *J. Biogeogr.* 46:833–844.
- Mcvay JD, Flores-Villela O, Carstens B. 2015. Diversification of North American natricine snakes. *Biol. J. Linn. Soc.* 116:1–12.
- Mebert K. 2008. Good species despite massive hybridization: Genetic research on the contact zone between the watersnakes *Nerodia sipedon* and *N. fasciata* in the Carolinas, USA. *Mol. Ecol.* 17:1918–1929.

- Nosil P. 2008. Speciation with gene flow could be common. *Mol. Ecol.* 17:2103–2106.
- Patton AH, Margres MJ, Epstein B, Eastman J, Harmon LJ, Storfer A. 2020. Hybridizing salamanders experience accelerated diversification. *Sci. Rep.* 10:1–12.
- Pease JB, Haak DC, Hahn MW, Moyle LC. 2016. Phylogenomics Reveals Three Sources of Adaptive Variation during a Rapid Radiation. *PLoS Biol.* 14:1–24.
- Peng C, Ren J, Deng C, Jiang D, Wang J, Qu J, Chang J, Yan C, Jiang K, Murphy RW, et al. 2020. The genome of Shaw’s sea snake (*Hydrophis curtus*) reveals secondary adaptation to its marine environment. Liu L, editor. *Mol. Biol. Evol.*:1–37.
- Petkova D, Novembre J, Stephens M. 2016. Visualizing spatial population structure with estimated effective migration surfaces. *Nat. Genet.* 48:94–100.
- Pettus D. 1958. Water Relationships in *Natrix sipedon*. *Copeia* 1958:207–211.
- Pettus D. 1963. Salinity and Subspeciation in *Natrix sipedon*. *Copeia* 1963:499–504.
- Pfeifer SP, Laurent S, Sousa VC, Linnen CR, Foll M, Excoffier L, Hoekstra HE, Jensen JD. 2018. The evolutionary history of Nebraska deer mice: Local adaptation in the face of strong gene flow. *Mol. Biol. Evol.* 35:792–806.
- Pickrell JK, Pritchard JK. 2012. Inference of Population Splits and Mixtures from Genome-Wide Allele Frequency Data. Tang H, editor. *PLoS Genet.* 8:e1002967.
- De Queiroz K. 2007. Species concepts and species delimitation. *Syst. Biol.* 56:879–886.
- R Core Team. 2020. R: A language and environment for statistical computing. R Foundation for Statistical Computing, Vienna, Austria. URL <https://www.R-project.org/>. Available from: <https://www.r-project.org/>
- Rambaut A, Drummond AJ, Xie D, Baele G, Suchard MA. 2018. Posterior summarization in Bayesian phylogenetics using Tracer 1.7. *Syst. Biol.* 67:901–904.
- Rasmussen AR, Murphy JC, Ompi M, Gibbons JW, Uetz P. 2011. Marine reptiles. *PLoS One* 6.
- Ronquist F, Teslenko M, Van Der Mark P, Ayres DL, Darling A, Höhna S, Larget B, Liu L, Suchard MA, Huelsenbeck JP. 2012. Mrbayes 3.2: Efficient bayesian phylogenetic inference and model choice across a large model space. *Syst. Biol.* 61:539–542.
- Rundle HD, Nosil P. 2005. Ecological speciation. *Ecol. Lett.* 8:336–352.
- Saidi D. 2012. Importance and role of cation exchange capacity on the physicals properties of the Cheliff saline soils (Algeria). *Procedia Eng.* 33:435–449.
- Savolainen O, Lascoux M, Merilä J. 2013. Ecological genomics of local adaptation. *Nat. Rev. Genet.* 14:807–820.
- Schild DR, Card DC, Adams RH, Jezkova T, Reyes-Velasco J, Proctor FN, Spencer CL, Herrmann HW, Mackessy SP, Castoe TA. 2015. Incipient speciation with biased gene flow between two lineages of

- the Western Diamondback Rattlesnake (*Crotalus atrox*). *Mol. Phylogenet. Evol.* 83:213–223.
- Schluter D. 2000. *The Ecology of Adaptive Radiation*. Oxford: Oxford University Press
- Scrucca L, Fop M, Murphy TB, Raftery AE. 2016. mclust 5: Clustering, Classification and Density Estimation Using Gaussian Finite Mixture Models. *R J.* 8:289–317.
- Slatkin M. 1987. Gene flow and the geographic structure of natural populations. *Science* (80-.). 236:787–792.
- Soltis DE, Morris AB, McLachlan JS, Manos PS, Soltis PS. 2006. Comparative phylogeography of unglaciated eastern North America. *Mol. Ecol.* 15:4261–4293.
- Stamatakis A. 2014. RAxML version 8: A tool for phylogenetic analysis and post-analysis of large phylogenies. *Bioinformatics* 30:1312–1313.
- Strickland JL, Parkinson CL, McCoy JK, Ammerman LK. 2014. Phylogeography of *Agkistrodon piscivorus* with Emphasis on the Western Limit of Its Range. *Copeia* 2014:639–649.
- Territo GP. 2013. Biogeography and Systematics of the *Nerodia clarkii/Nerodia fasciata* Clade in Florida.
- Tigano A, Friesen VL. 2016. Genomics of local adaptation with gene flow. *Mol. Ecol.* 25:2144–2164.
- Townsend TM, Alegre RE, Kelley ST, Wiens JJ, Reeder TW. 2008. Rapid development of multiple nuclear loci for phylogenetic analysis using genomic resources: An example from squamate reptiles. *Mol. Phylogenet. Evol.* 47:129–142.
- Tuanmu MN, Jetz W. 2014. A global 1-km consensus land-cover product for biodiversity and ecosystem modelling. *Glob. Ecol. Biogeogr.* 23:1031–1045.
- USFWS. 2008. Atlantic Salt Marsh Snake (*Nerodia clarkii taeniata*) 5-Year Review: Summary and Evaluation. U.S. Fish and Wildlife Services. Jacksonville, Florida USA.
- Wang IJ, Bradburd GS. 2014. Isolation by environment. *Mol. Ecol.* 23:5649–5662.
- Wickham H. 2016. *ggplot2: Elegant Graphics for Data Analysis*. New York: Springer-Verlag
- Wilke CO. 2020. ggridges: Ridgeline Plots in “ggplot2.” Available from: <https://cran.r-project.org/package=ggridges>
- Wood DA, Vandergast AG, Lemos Espinal JA, Fisher RN, Holycross AT. 2011. Refugial isolation and divergence in the narrowheaded gartersnake species complex (*Thamnophis rufipunctatus*) as revealed by multilocus DNA sequence data. *Mol. Ecol.* 20:3856–3878.
- Wright S. 1931. Evolution in Mendelian Populations. *Genetics* 16:97–159.
- Yeaman S, Whitlock MC. 2011. The genetic architecture of adaptation under migration-selection balance. *Evolution* (N. Y). 65:1897–1911.
- Zhang X, Wen H, Wang H, Ren Y, Zhao J, Li Y. 2017. RNA-Seq analysis of salinity stress-responsive transcriptome in the liver of spotted sea bass (*Lateolabrax maculatus*). *PLoS One* 12:1–18.

Fig. 1. Distribution map for the five subspecies within the *Nerodia fasciata-clarkii* complex in Florida.

Colors are maintained throughout the manuscript. Photo of *N. c. taeniata* by G. Territo.

Fig. 2. *DAPC* population structure for 118 snakes across Florida. (A) $K=2$ shows that genetic clustering is similar to the species distributions (see fig. 1). Population structure at (B) $K=5$ shows that genetic clustering is similar to subspecies distributions (see fig. 1). The best supported *DAPC* model, (C) $K=6$, separates the *N. c. compressicauda* population into central and southern groups. (D) At $K=7$, the eastern and western *N. c. compressicauda* clades separate. Inset density and scatter plots represent separation along discriminant axes and the DA eigenvalues describe how much discriminating ability the model possesses. Not all 118 points may be visible in maps since some points overlap.

Fig. 3. (A) *conStruct* population structure and admixture at $K=2$ with additional $K=5$ admixture plot showing little structure at $K=5$. (B) Estimated effective migration surface (*EEMS*) for the *N. fasciata-clarkii* complex. High migration is represented by shades of blue; low migration is represented by red-orange shades. *EEMS* demonstrates increased gene flow within and decreased gene flow between the coastal and inland populations. Photos of *N. c. clarkii* and *N. f. fasciata* by K. Wray.

Fig. 4. *SVDquartets* inferred phylogeny with *conStruct* and *DAPC* results annotated. Nodal support is represented by color and size with large, black dots representing 100% bootstrap support and small, white points representing 0%. See supplementary fig. S7 for a cladogram with numerical support values. *SVDquartets* and *Treemix* species tree are also shown for $K=5$ with three migration edges leading from *N. fasciata* to *N. clarkii*, particularly from *N. f. pictiventris* to *N. c. compressicauda*. *HyDe* similarly detected three significant hybridization events, position of hybridization edges on branches is arbitrary.

Fig. 5. Violin plot demonstrating the differences in cation exchange capacity of the soil – used as a metric of salinity – between *N. fasciata* and *N. clarkii* based on *DAPC* assignment at $K=2$. Regression of *conStruct* admixture proportion at $K=2$ (proportion assigned to *N. fasciata*) with cation exchange capacity of the soil. Points are colored by *DAPC* assignment at $K=6$.

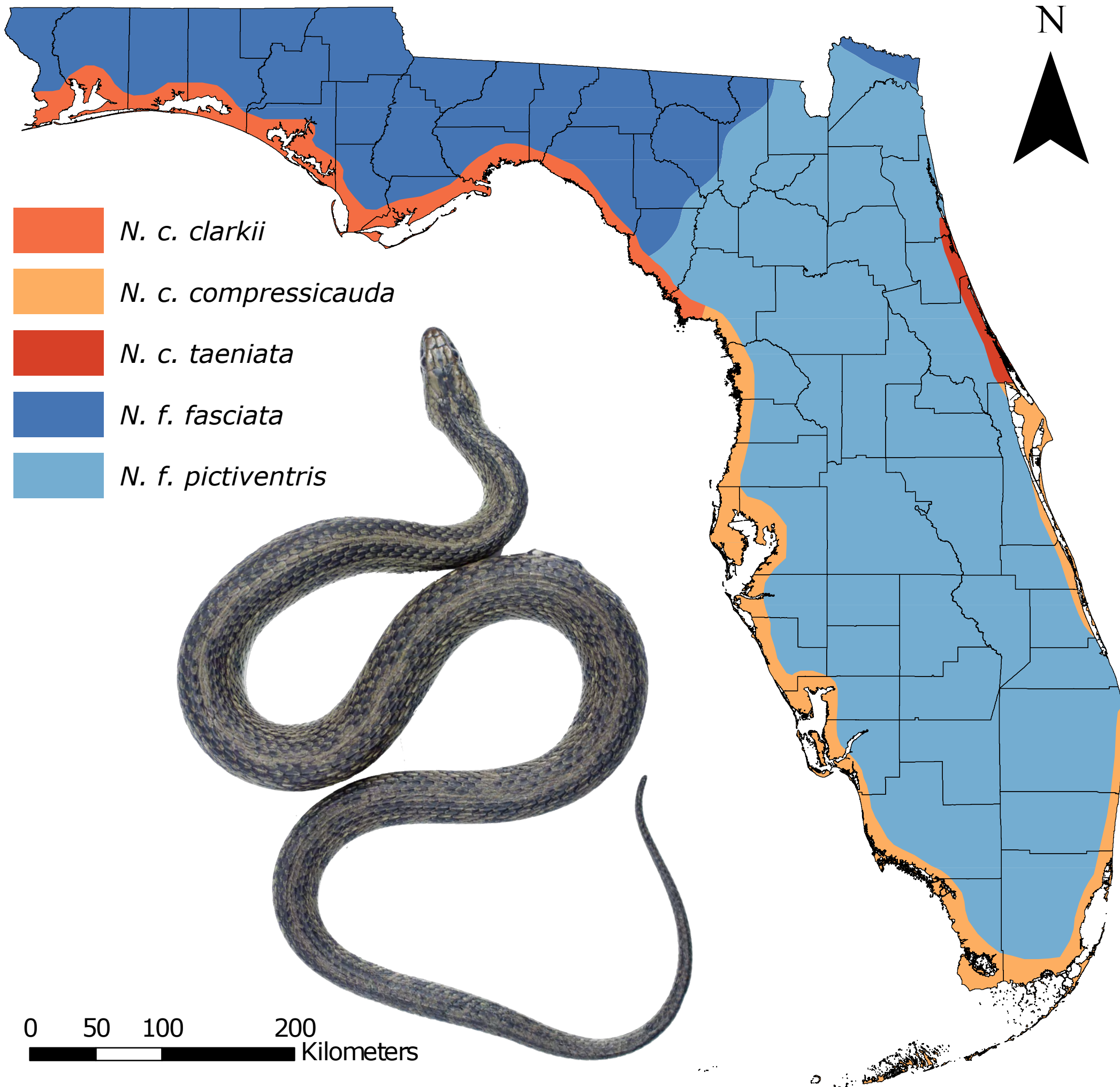
Fig. 6. Left: Network generated by *ShinyGO* of all significantly enriched GO terms for genes shared across *BayeScan* scans. Two nodes are connected if they share greater than 20% of their genes. Node size corresponds to size of the gene sets and edge thickness correspond to the number of overlapped genes. The colored envelopes represent modules with dense nodal connections, but sparse connections to other modules. Right: Genes associated with ion, cation, and transmembrane transport which are likely related to osmoregulatory adaptations associated with coping with saline environments in *N. clarkii*.

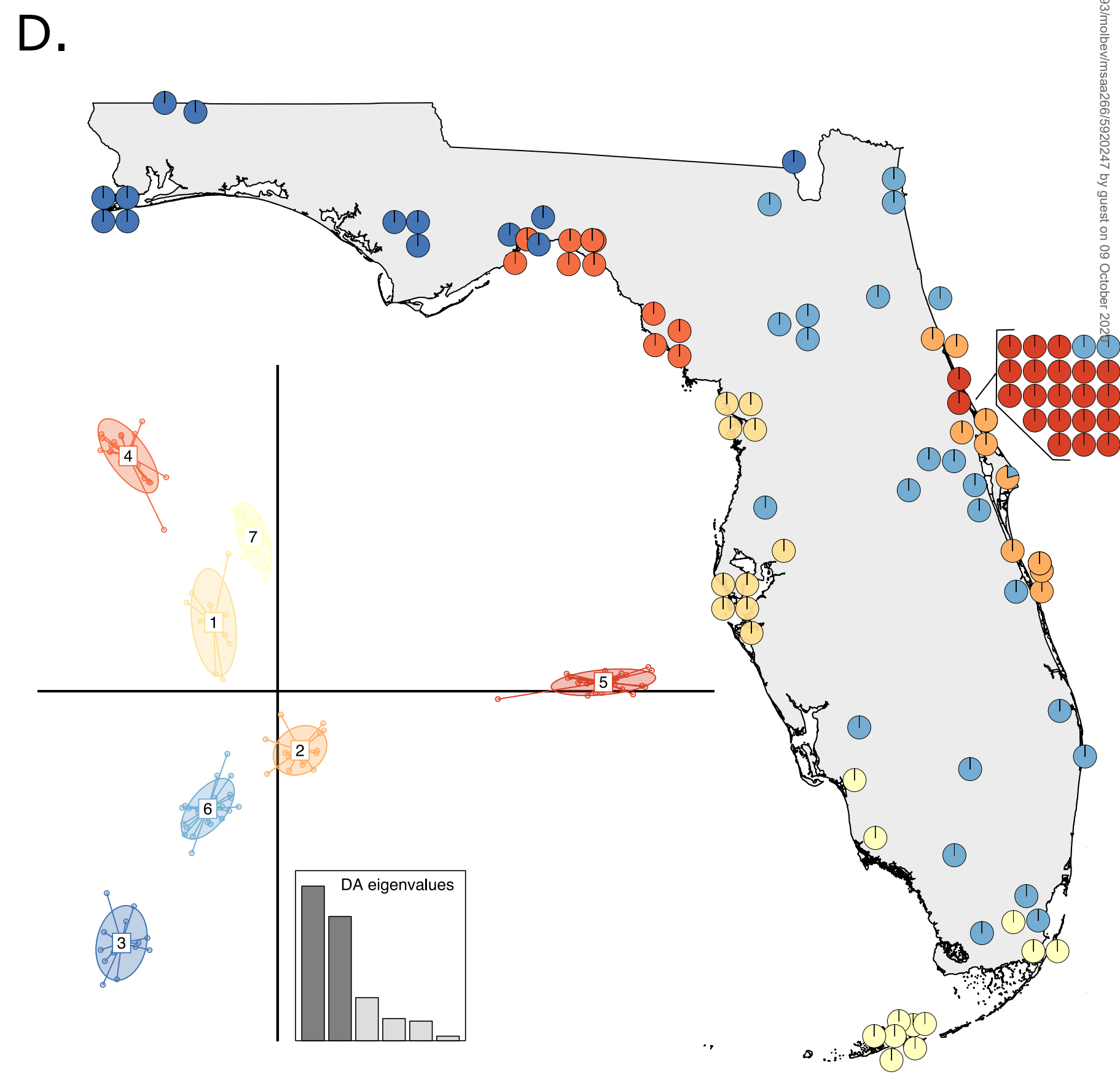
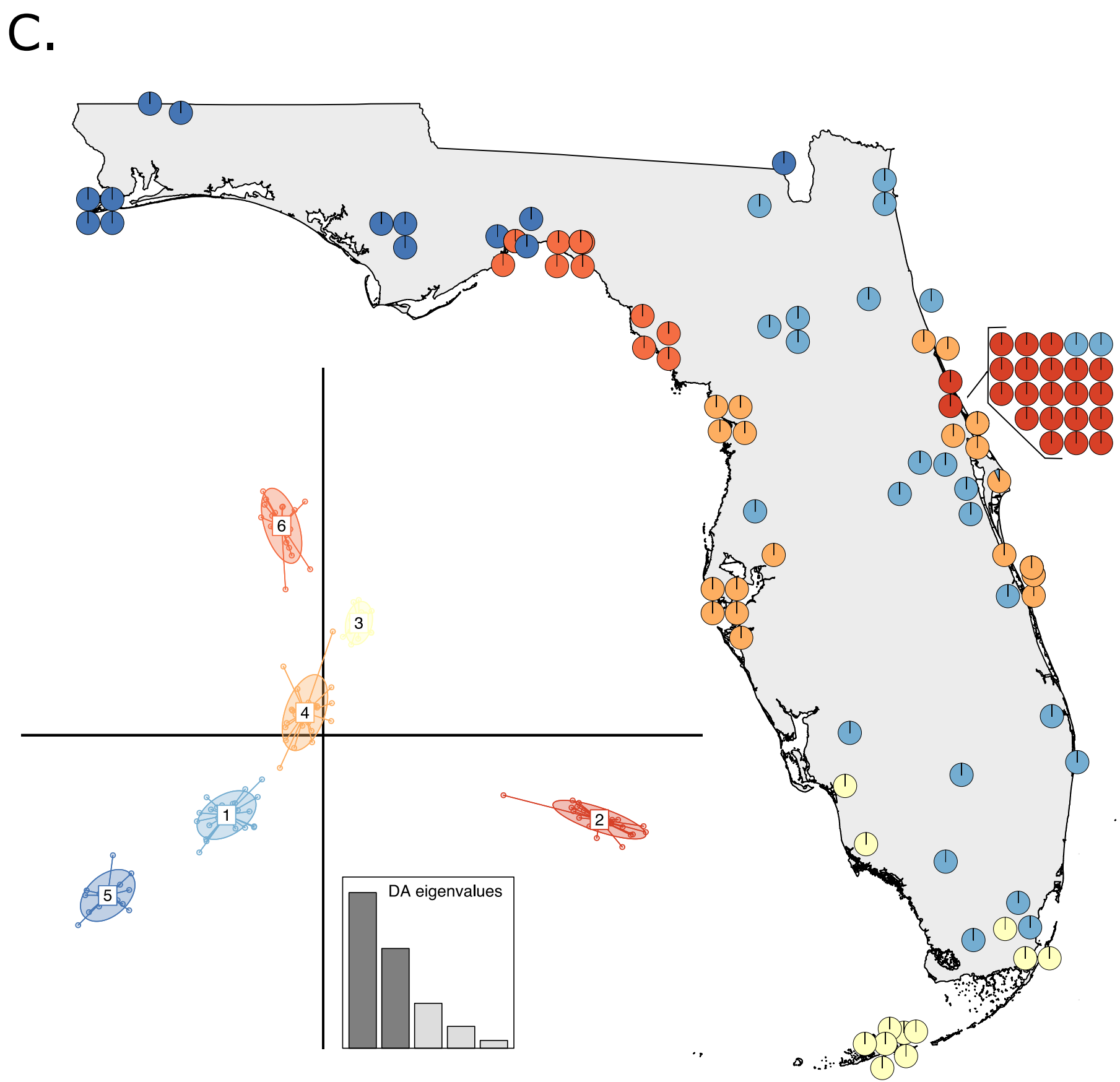
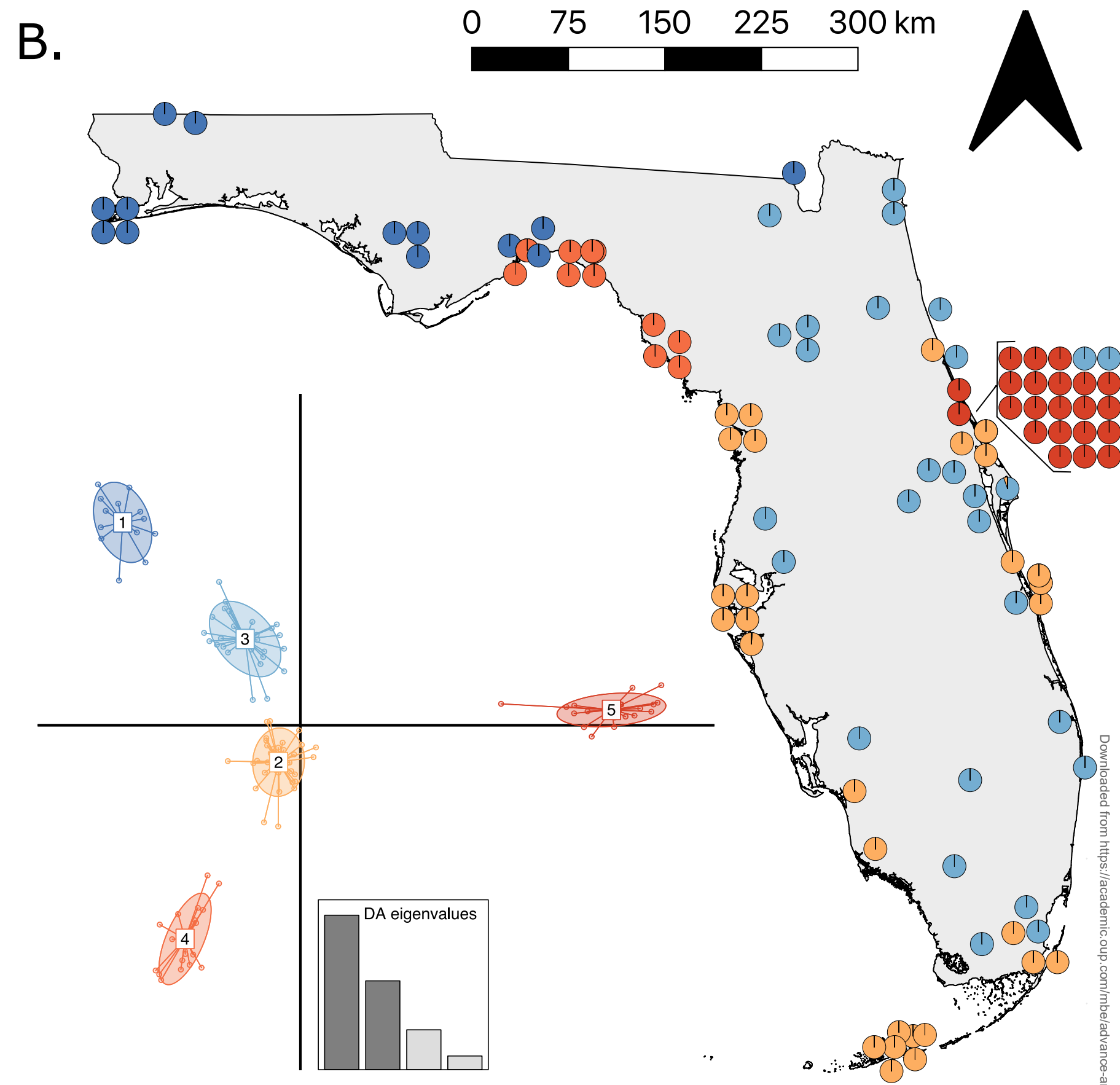
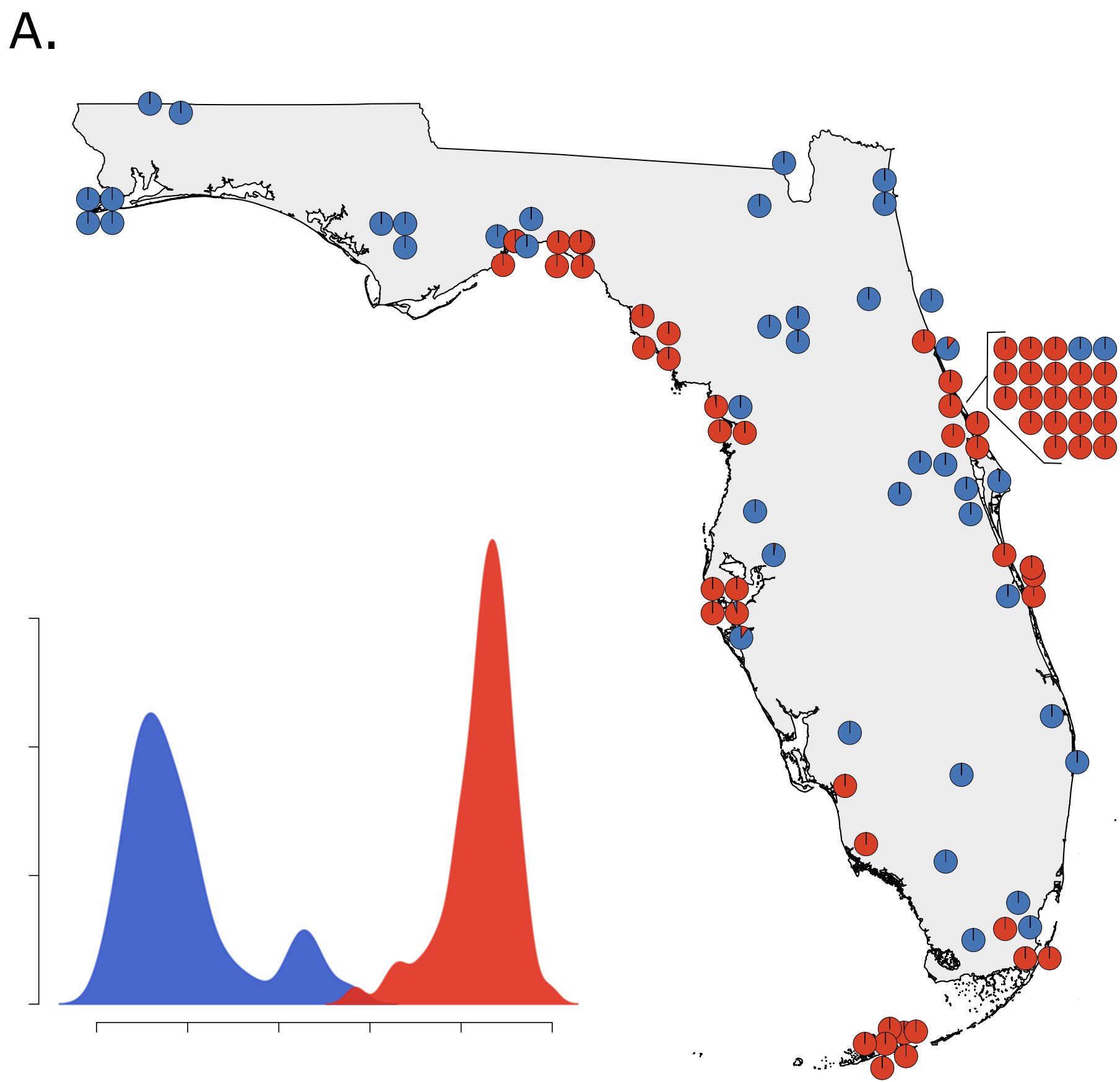
Supplementary table S1. Sample database including University of Florida Museum numbers and GenBank accession numbers.

Supplementary table S2. Nucleotide substitution models and partitioning schemes as determined in PartitionFinder v. 2.1.1 for mitochondrial and nuclear genes

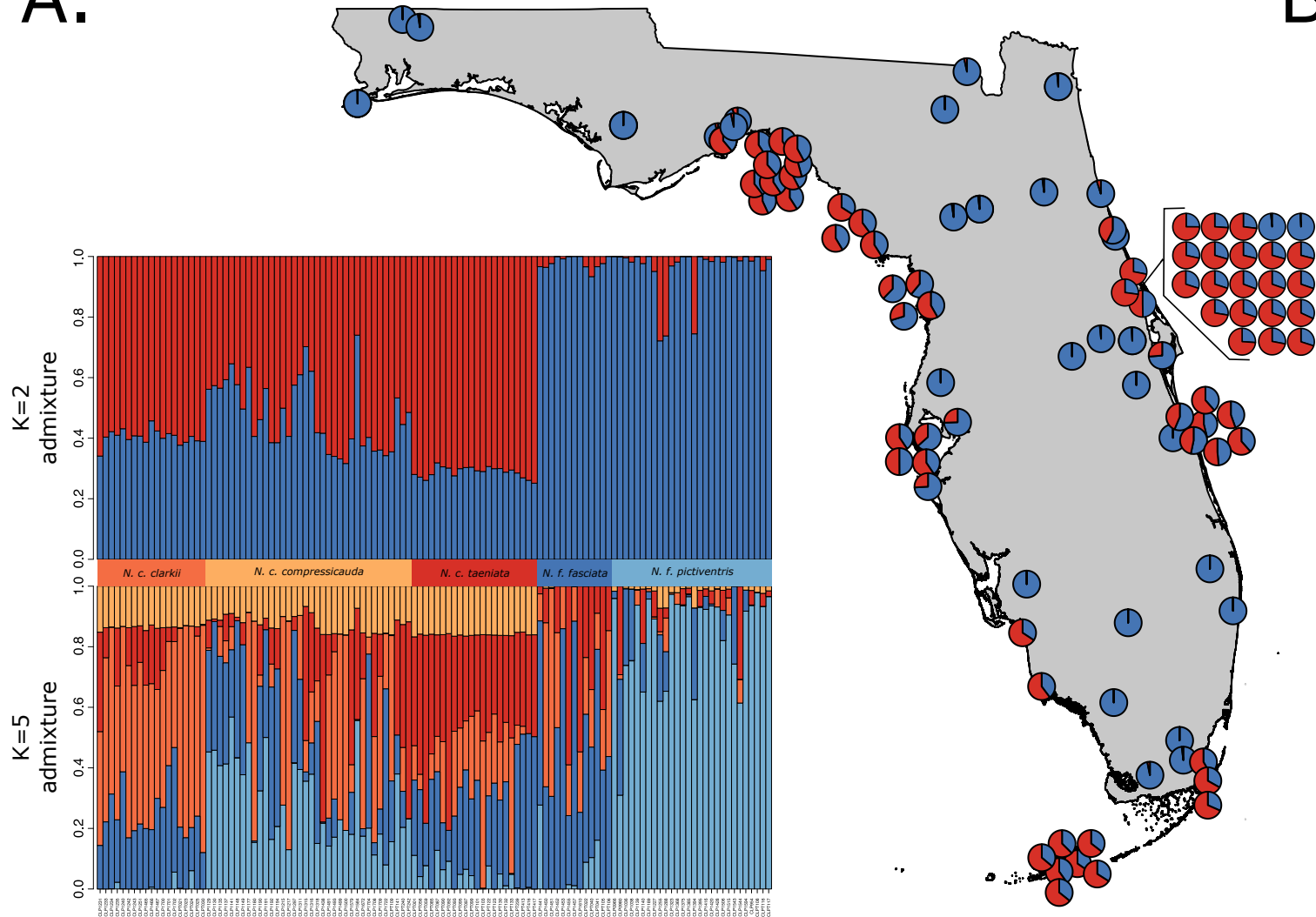
Supplementary table S3. Results from *BayeScan* including SNP number, q-value, F_{ST} , allele counts for each population, alternate allele frequency, and allele frequency differences (AFD).

Supplementary table S4. List of genes in the *Thamnophis elegans* genome (NC_045558.1) which had *BLAST* search matches to loci found to be outliers by *BayeScan* between *Nerodia clarkii* and *Nerodia fasciata*.



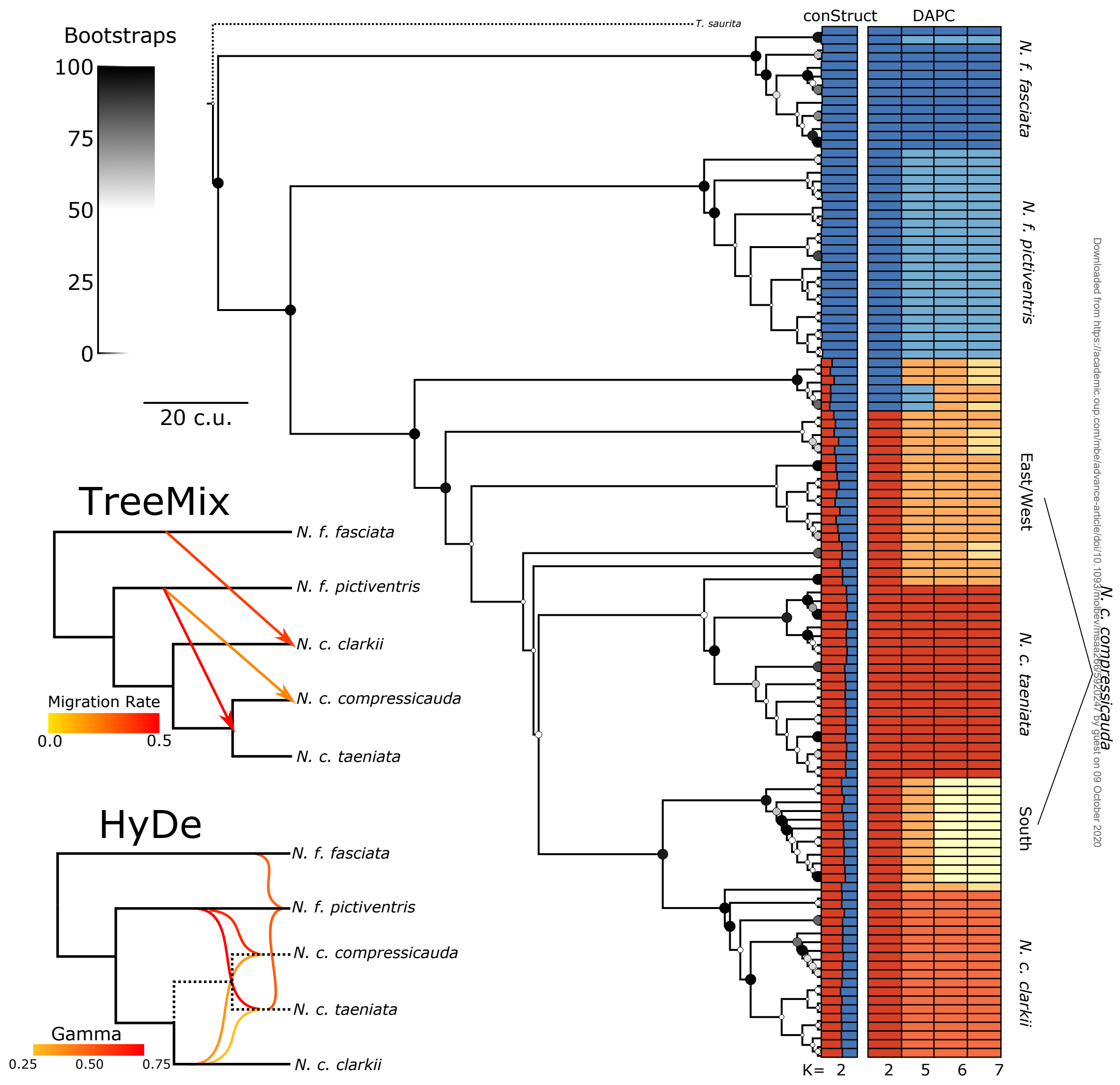


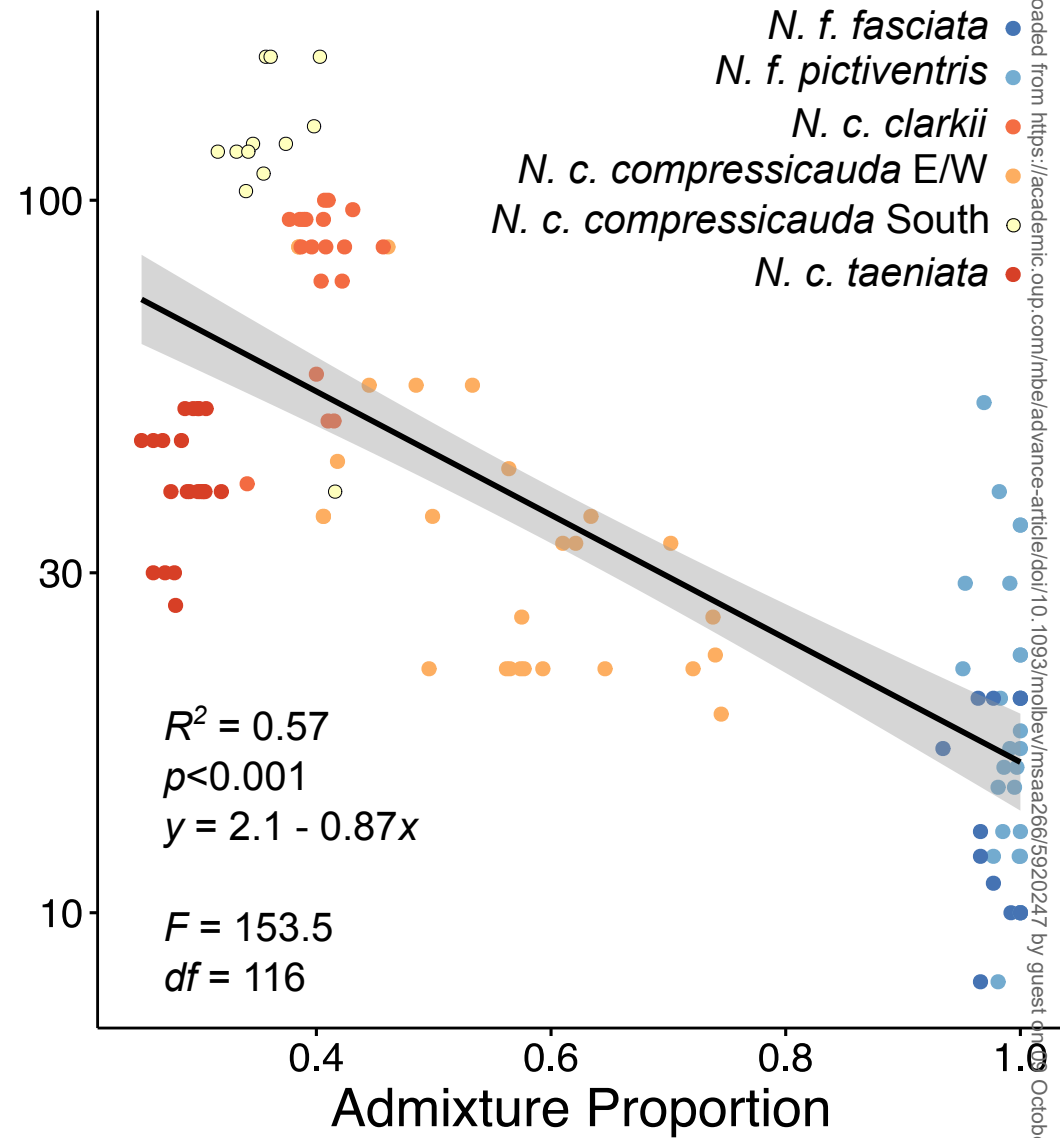
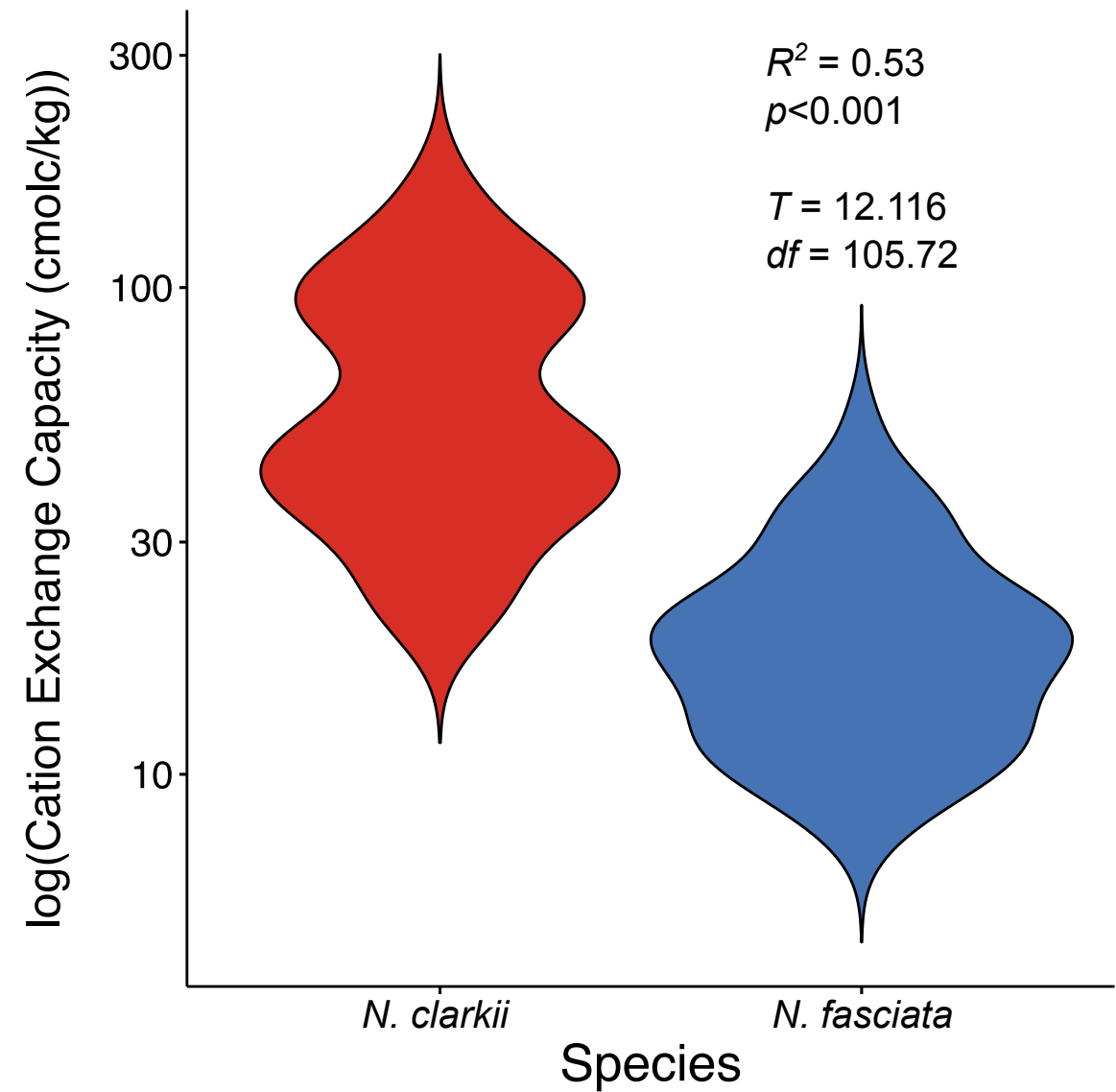
A.

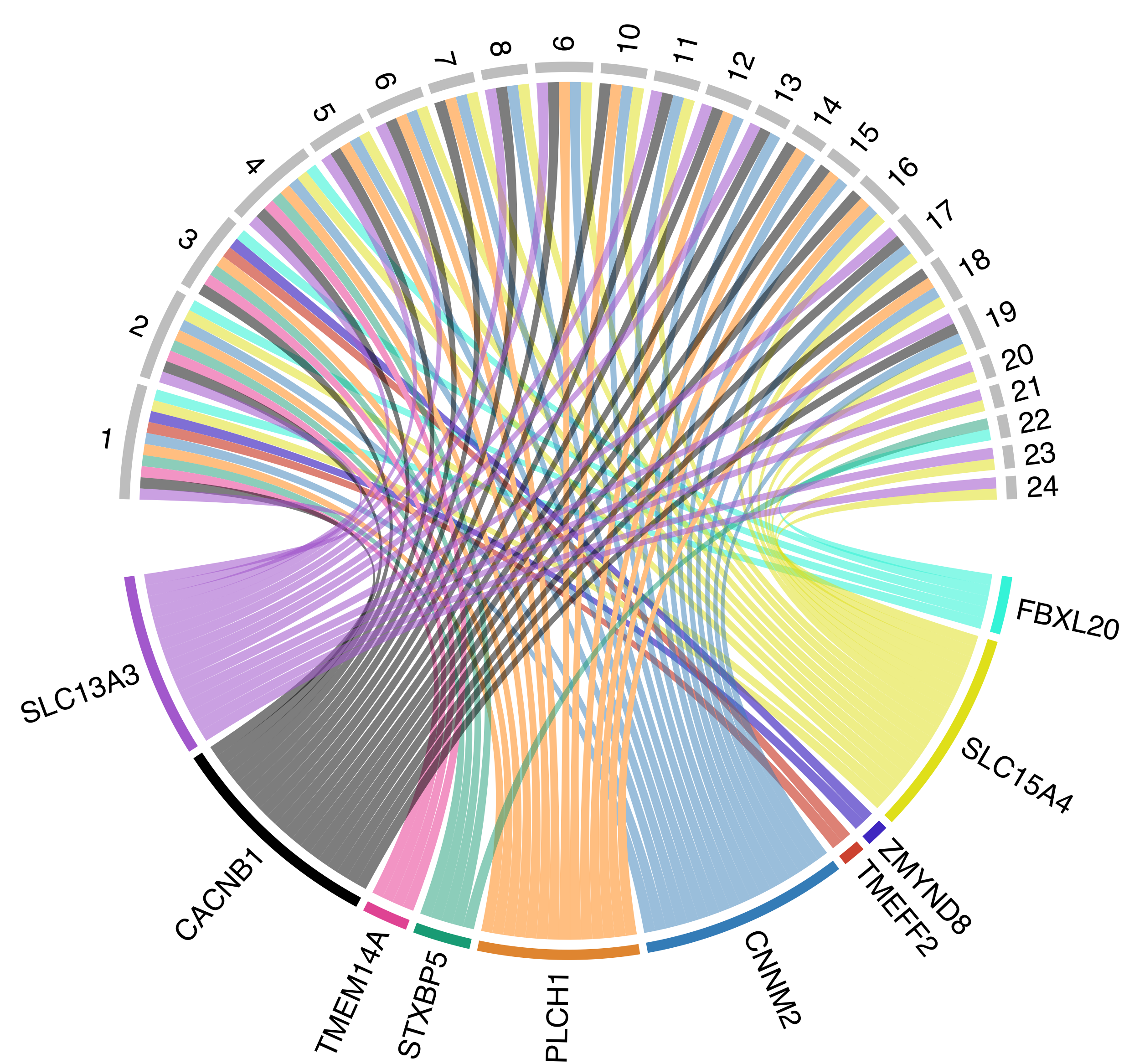
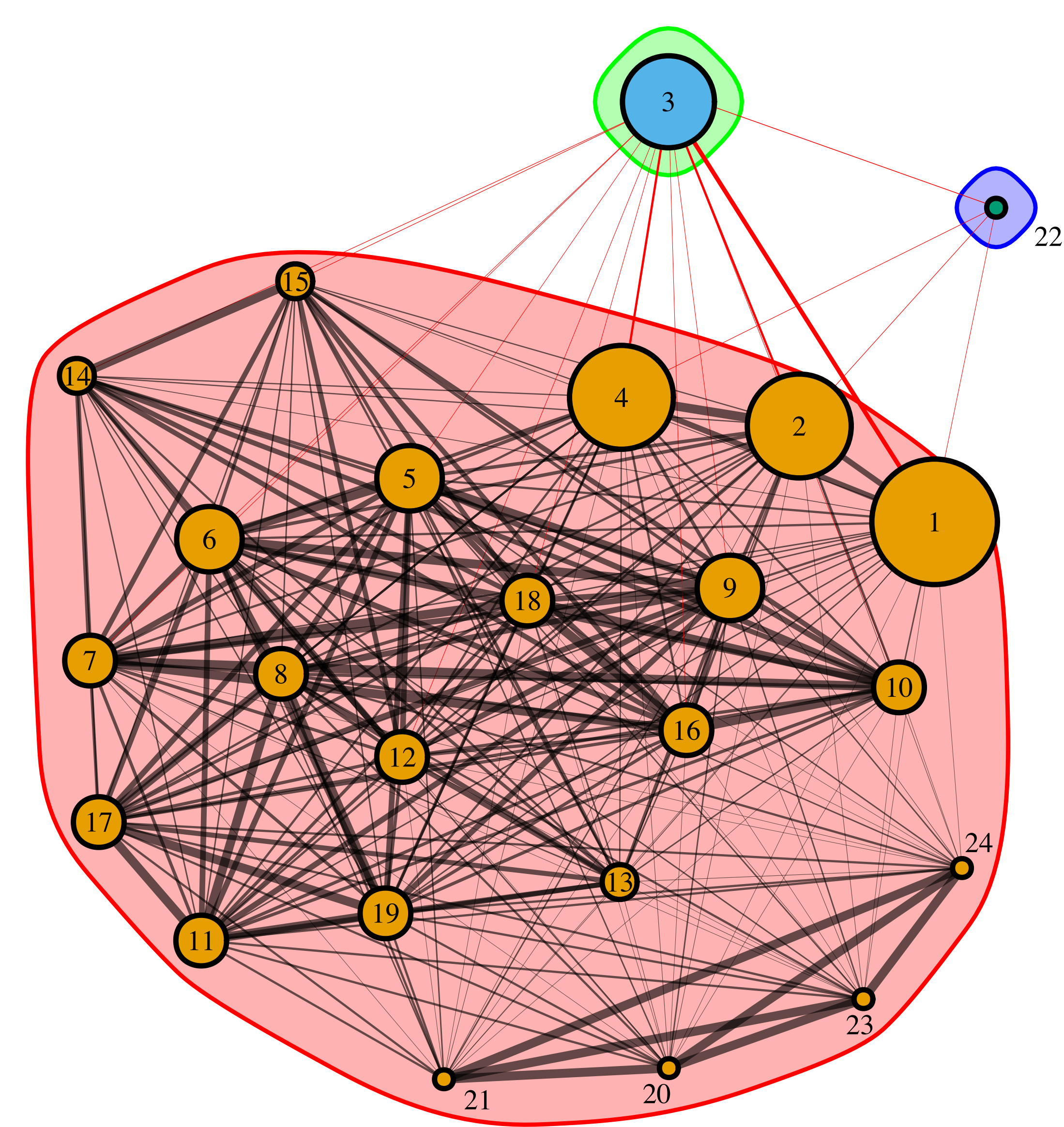


B.









- 1 Localization
- 2 Establishment of localization
- 3 Regulation of localization
- 4 Transport
- 5 Transmembrane transport
- 6 Ion transport
- 7 Ion transmembrane transport
- 8 Ion transmembrane transporter activity
- 9 Cation transport
- 10 Cation transmembrane transport
- 11 Cation transmembrane transporter activity
- 12 Metal ion transport
- 13 Metal ion transmembrane transporter activity
- 14 Divalent metal ion transport
- 15 Divalent inorganic cation transport
- 16 Inorganic cation transmembrane transport
- 17 Inorganic cation transmembrane transporter activity
- 18 Inorganic ion transmembrane transport
- 19 Inorganic molecular entity transmembrane transporter activity
- 20 Carboxylic acid transmembrane transporter activity
- 21 Organic acid transmembrane transporter activity
- 22 Regulation of exocytosis
- 23 Solute:cation symporter activity
- 24 Symporter activity